Oncogenic Stress is a Novel Immunogenic Signal Driven by the Unfolded Protein Response and Detected by Neutrophils

Antoine Debiesse[1], Lyvia Moudombi[1], Aurélien Voissière[1], Leïla Lefèvre[1,2], Marine Malfroy[1,3], Iryna Moskalevska[4], Manuela Pereira Abrantes[1,5], Hélène Vanacker[1,6], Margaux Hubert[7], Roxane Pommier[8], Cassandra Assaf[1], Emmanuelle Jacquet[1,9], Marie Laurent[1,6], Sara Belluco[10], Nadège Goutagny[1,11], Virginie Petrilli[1], Julien Cherfils-Vicini[4], Christophe Caux[1,12], Nathalie Bendriss-Vermare[1,12$] and Marie-Cécile Michallet[1$].

[1]Centre de Recherche en Cancérologie de Lyon (CRCL), Centre Léon Bérard, Université de Lyon, Université Claude Bernard Lyon 1, INSERM 1052, CNRS 5286, 69008 Lyon, France

[2]Current address: Paris Centre University Hospital Infectious Diseases Stewardship team, AP-HP, Paris, France

[3]Current address : Etablissement Français du Sang, Besançon, France

[4]Université Côte d'Azur, Centre National de la Recherche Scientifique (CNRS) UMR7284, Institut National de la Santé et de la Recherche Médicale (INSERM) U1081, Institute for Research on Cancer and Aging, Nice (IRCAN), Nice 06107, France

[5]Current address: Bayer HealthCare SAS, Medical Affairs, Lille 59000, France

[6]Department of clinical oncology, Centre Léon Bérard, Lyon, France

[7]Current address: Sanofi, Marcy L'Etoile, France

[8]Synergie Lyon Cancer, 'Gilles Thomas' Bioinformatics Platform, Lyon, France

[9]Department of clinical oncology, CHU Grenoble Alpes, Grenoble, France

[10]VetAgroSup, Marcy L'Etoile, France

[11]Current address : Biomérieux, Marcy L'Etoile, France

[12]Laboratory for Immunotherapy of Cancer of Lyon (LICL), Centre de Recherche en Cancérologie de Lyon, Centre Léon Bérard, Lyon, France

$These authors jointly supervised this work

Corresponding author Email: marie-cecile.michallet@lyon.unicancer.fr

KEYWORDS

Oncogenic Stress - Immunosurveillance - Neutrophils - Breast Cancer

ABSTRACT

Cellular transformation is initiated by a driver mutation, resulting in the abnormal expression of an oncogene or the loss of a tumor suppressor gene in a normal cell. This event leads to oncogenic stress (OS), describing a disruption of cellular homeostasis which activates stress response pathways and transcriptomic programs that can either promote tumor development or trigger intrinsic safeguards such as senescence or apoptosis. While the immunogenicity of senescent cells is well established, the immunogenic potential of cells at the early OS stage and the mechanisms by which they are sensed by the immune system remain unknown. We developed an original *in vitro* OS model using primary human mammary epithelial cells to investigate this process. Our results show that OS cells display an immunoactive secretome associated with OS (SOS), as well as immunogenic membrane ligands. Intrinsically, OS cells activate the PERK and IRE1 branches of the unfolded protein response (UPR) that regulate their immunogenic features. Extrinsically, we demonstrated that neutrophils can detect OS-induced immunogenic signals, leading to their recruitment and their activation in co-culture *in vitro*. We validated this observation in two spontaneous murine models of breast cancer, where the earliest preneoplastic stages exhibit both UPR activation in epithelial cells and neutrophil infiltration. Altogether, our work identifies OS as the first immunogenic event in carcinogenesis and neutrophils as the first immune cell involved in immunosurveillance, paving the way for potential therapeutic approaches intercepting early steps of tumorigenesis.

INTRODUCTION

Tumorigenesis is initiated by the abnormal expression of an oncogene or the loss of a tumor suppressor gene in a normal cell. This event induces oncogenic stress (OS), which represents the first challenge that a cell must overcome to develop into a tumor. If cells fail to adapt to OS, intrinsic safeguard mechanisms are triggered, such as Oncogene-Induced Senescence (OIS)[1]. OIS is well characterized for its immunomodulatory potential[2], primarily through the Senescence-Associated Secretory Phenotype (SASP), a hallmark of senescent cells[3]. SASP involves the secretion of pro-inflammatory cytokines, chemokines, growth factors, and proteases[2,4–6]. This secretory profile promotes the recruitment of immune cells, including neutrophils, macrophages, and NK cells, to the site of senescent cells[7,8], facilitating their clearance *in vivo*[9]. Mechanistically, the chemokine CXCL14, secreted by p21-overexpressing senescent cells, was shown to recruit M1 macrophages and activate cytotoxic T cells, contributing to the efficient immune-mediated clearance of senescent cells *in vivo*[10]. Alongside this secretory activity, senescent cells undergo surface modifications, including the upregulation of immunogenic membrane ligands such as NKG2D ligands[11,12] and antigen-presenting molecules like MHC class I[13–15], which enhance the recognition and elimination of senescent cells by engaging NK cells and cytotoxic T cells[8,13,16]. Although alterations in the surfaceome of senescent cells can enhance immune surveillance, they also contribute to immune escape through the expression of senescence immune checkpoints. Recent studies have shown that senescent cells impede their own clearance by CD8 T cells through the expression of programmed cell death ligand 1 (PD-L1)[17]), PD-L2[18], and HLA-E, which is known to hinder NK cell surveillance[19]. Additionally, we have expanded the family of senescence immune checkpoints by discovering that both human and mouse senescent cells overexpress the disialylated ganglioside GD3, which prevents NK cell degranulation and interferon-gamma (IFNγ) production[20].

The knowledge of immune surveillance mechanisms occurring at early/OS stages, before any sign of senescence remains largely hypothetical, due to the inability in accessing human biological samples and the lack of appropriate preclinical mouse models. We therefore hypothesize that the OS, that precedes OIS, also manifests an immunogenic potential leading to the recruitment and activation of immune cells ultimately resulting in the elimination of OS cells. We addressed this hypothesis in the context of breast cancer, as it represents a complex and heterogeneous disease that is still the primary

cause of cancer-related mortality among women globally[21], and where immunotherapy treatments are still not effective in all patients[22].

In this study, we developed innovative and complementary *in vitro* (human mammary epithelial cells) and *in vivo* (MMTV-Neu and BLG-cre; BRCA1f/f; p53+/-) breast cancer models to investigate immune surveillance during OS. We identified that OS in breast epithelial cells induces immunogenicity driven by a secretome (SOS) and membrane ligands. Mechanistically, we showed that OS triggers the activation of unfolded protein response (UPR) pathways, which partially regulate these immunogenic features. Additionally, we demonstrated that OS is sensed by and activates neutrophils. Altogether our results demonstrated that oncogenic stress (OS) acts as the earliest immune alert signal, detected by neutrophils which serve as the first line of defense against tumor progression.

RESULTS

The Oncogenic Stress (OS) is the first immunogenic state in cellular transformation

To study the Oncogenic Stress (OS), we have developed an original *in vitro* model using primary immortalized human mammary epithelial cells (HMEC) with doxycycline (dox)-inducible expression of $HRas^{G12V}$ (herein referred to as HMEC-HRas), which is relevant to the $HER2^{+}$ breast cancer[23] (see Materials and methods section and **Fig 1a**). Upon dox treatment, HMEC-HRas overexpress Ras starting from day 2 (d2), with levels increasing thereafter, accompanied by the upregulation of ERK phosphorylation (**Fig 1b**). Additionally, microarray-based transcriptomic analysis revealed an elevated ssGSEA score for the HRas signature in treated-cells at d3 and d5, confirming the activation of the HRas signaling pathway (**Fig 1c**). At d5 of culture, HMEC-HRas express several intrinsic senescence features such as morphological changes (**Fig S1a-b**), a limitation of proliferation (**Fig S1c**), the cell-cycle arrest (**Fig S1d**), *b*-galactosidase activity (**Fig S1e**) and the transcriptional downregulation of the DNA damage response (DDR)[24] (**Fig S1f**). Then, at d5 HMEC-HRas exhibit a SASP (**Fig S1g-h**) and senescence signatures from public datasets[25,26] (**Fig S1i**). Collectively, our findings highlight that by day 5, HRas effectively induces a state of oncogene-induced senescence (OIS) in HMEC, suggesting that the cells had previously undergone OS. In contrast with d5, HMEC-HRas at d3 conceal any signs of intrinsic senescence features at d3 (**Fig S1a-f**) whereas experienced cellular stress, as evidenced by a significant enrichment of a stress response signature (**Fig 1d**), as well as the expression of NKG2D ligands (NKG2D-L - ULBP2-5-6) that have been shown to be expressed by stressed[27] and senescent[28] cells - **Fig 1e; Fig S1j-k**). After determining that the cells were undergoing OS at d3, characterized by a stress response and the absence of intrinsic senescence features, we focused on the immunogenicity of OS cells.

Performing differentially expressed genes (DEGs) analysis on HRas-induced OS HMEC compared to untreated HMEC (Ctl), we showed that OS cells upregulated 183 genes including 35 (19%) associated with secreted proteins, 46 (25%) related to plasma membrane proteins, 9 (5%) that are both secreted and plasma membrane-bound, and 93 (51%) linked to proteins localized in other subcellular compartments (cytosol, ER, etc. – **Table S1** and **Fig 1f,** Uniprot database (**https://www.uniprot.org/**)). The top 10 DEGs of the secreted proteins' group contain several immunogenic chemokines (*cxcl8/il-8*, *cxcl3*, *cxcl1* and *cxcl2*) and cytokines (*csf2*) (**Fig 1g; Fig S1g**) that were also upregulated at the protein level as quantified in the HRas-induced OS HMECs supernatant by ELISA (**Fig 1h**). Regarding type I

interferons (IFN), which are highly immunogenic molecules typically found in the SASP[29,30], we detected the enrichment of a type I-IFN signature (**Fig 1i**) and the expression of interferon-stimulated genes (ISGs - **Fig 1j**) in our transcriptomic data at the OS stage. Among membrane ligands, in addition to NKG2D-L which are also noted for their immunogenic potential in promoting the elimination of senescent tumor cells by NK cells[8], we identified an increase of *icam1* in the DEG (**Table S1, Fig S1l**), confirmed at the protein level in HMEC-HRas (**Fig 1k, left panel**). PD-L1 (*cd274*), which is also known to be regulated by the Ras pathway[31] and expressed by senescent cells[17], is overexpressed by HMEC-HRas in the transcriptomic data (**Table S1, Fig S1m**) as well as by flow cytometry (**Fig 1k, right panel; Fig S1n**). Taken together, our findings suggest that cells undergoing an HRas-induced OS are highly immunogenic due to their immunoactive Secretome (SOS) and the expression of innate immune-related membrane ligands.

HRas-induced OS leads to the activation of the Unfolded Protein Response

Emerging evidence points to the unfolded protein response (UPR)[32] (**Fig S2a**), triggered by ER stress, could be another potential driver of senescence[33]. Notably, HRas-induced OIS in primary mouse keratinocytes[34], primary human melanocytes[35] and human breast adenocarcinoma cell line[36] is marked by the activation of the UPR. Consistent with these studies, we showed that HRas-induced OIS in primary mammary epithelial cells appears to trigger ER stress (**Fig S2b**), activating the UPR and more specifically the inositol-requiring enzyme 1 (IRE1) and protein kinase RNA-like ER kinase (PERK) branches (**Fig S2c-d**), while activating transcription factor 6 (ATF6) seems to be less involved (**Fig S2c**). In fact, the ER stress is already detected at d3 when cells enter in OS (**Fig 2a**). Furthermore, OS cells show enriched IRE1- and PERK-target signatures, validated by western blot showing IRE1 overexpression and PERK/EIF2A phosphorylations, with no change in ATF6 (**Fig 2b-c**). Additionally, we confirmed the increased expression of IRE1 (spliced form of *xbp1* (*xbp1*s), *dnajb9*, *hrd1* and *herpud* - **Fig 2d**) and PERK (*chop* and *ppp1r15a* - **Fig 2e**) target genes in HMEC-HRas at d3, compared to the control cell line (HMEC overexpressing an inducible GFP construct, see Materials and methods section and **Fig S2e-f**). We also demonstrated that physiological activation of the Ras signaling pathway by adding epidermal growth factor (EGF)[37,38] at different concentrations (5, 20 and 100 ng/mL) and in kinetics (0.5, 6, 12, 24 and 72h) (**Fig S2g-h**) in the culture medium of HMEC did not activate the UPR pathways by monitoring the expression of *dnajb9*, *chop* and *ppp1r15a* (**Fig S2i**). Lastly, considering that oncogenic Ras may reprogram glucose metabolism by increasing its uptake[39,40], and that ER stress can

be a consequence of glucose deprivation[34,41–43], we quantified glucose concentration in HMEC-HRas medium showing no starvation (**Fig S2j-k**). Moreover, glucose supplementation had no effect on the level of activation of the IRE1 and PERK pathways (**Fig S2l**), demonstrating that the UPR activation is therefore a consequence of the OS at d3. Taken together, we demonstrated that the UPR activation is an early feature of cellular transformation occurring as soon as the HRas-induced OS stage.

Immunogenic features of HRas-induced OS cells are regulated by IRE1 and PERK pathways

To assess the involvement of the PERK and the IRE1 pathways in regulating the immunogenic potential of HRas-induced OS cells, we added pharmacological inhibitors GSK-2606414 (PERK) and 4µ8c (IRE1) in HRas-induced OS culture during the last 24 hours (**Fig 3a; Fig S3a**). We validated inhibitors' specificity, with decreased expression of PERK-target genes (*chop* and *ppp1r15a*) in the presence of GSK-2606414, and reduced expression of the IRE1-target gene *dnajb9* with 4µ8c (**Fig S3b**). Treatment with GSK-2606414 had no impact on OS-induced secretion of IL8, GM-CSF, and CXCL1 (**Fig 3b**) whereas 4µ8c inhibited significantly the secretion of these three cytokines/chemokines by HRas-induced OS cells (**Fig 3c**). Both inhibitors did not impact significantly the basal secretions by untreated HMEC (**Fig 3b-c**). Regarding membrane-bound immunogenic markers, ICAM1 expression is unaffected by the inhibitors whereas the basal expression of PD-L1 is decreased by the 4µ8c treatment. For ULBP2-5-6, PERK inhibition reduced their basal expression, while IRE1 inhibition amplified the OS-induced expression (**Fig. 3d-e**). In summary, these results highlight that HRas-induced OS immunogenic features are tightly regulated by the UPR pathways, with an exclusive control of the secretome by IRE1 and the involvement of both PERK and IRE1 branches in the regulation of some membrane-bound immunogenic markers.

HRas-induced OS immunogenic cells trigger neutrophil recruitment and activation

As the SOS is composed of numerous inflammatory chemokines and cytokines known to recruit immune cells, we investigated whether HRas-induced OS cells can recruit immune cell population(s). Using lysed whole blood from healthy donors, as a source of immune cell populations (lymphoid and myeloid cells) we performed 3h transwell assays in the presence of supernatants of HRas-induced OS cells or untreated cells (**Fig 4a**). Interestingly, the only immune population significantly recruited by the HRas-induced OS supernatant are the neutrophils (**Fig 4a**). This selectivity was confirmed using peripheral blood mononuclear cells (PBMCs) lacking neutrophils (**Fig S4a**) and purified neutrophils demonstrating

a direct effect of HRas-induced OS supernatant on their migration (**Fig 4b**). Next, we evaluated neutrophil recruitment *in vivo* using a matrigel plug assay[20] (**Fig S4b**). We first validated *in vitro* that the matrigel had no impact on kinetics of HRas overexpression and activation (**Fig S4c**), on HMEC proliferation (**Fig S4d**), and on the secretome production (**Fig S4e**). Then we engrafted at d0 matrigel-enriched with dox or not (control) and containing inducible HMEC in nude mice, and we harvested the cells at d3 (OS - **Fig 4c**). After dissociation of the matrigel plug, we showed a selective increase in terms of frequency and number of neutrophils among immune cells in OS condition compared to untreated condition *in vivo* (**Fig 4d**), while the frequency and number of immune cells among viable cells remained unchanged (**Fig S4f**). We next aimed to evaluate whether HRas-induced OS cells activate neutrophils. Using neutrophils stimulated by HRas-induced OS supernatant, we first showed potent STAT5 phosphorylation downstream of GM-CSFR with an almost 2-fold increase compared to control (**Fig 4e**), associated to a significant increase in neutrophil producing reactive oxygen species (ROS - **Fig 4f**). Last, neutrophils co-cultured with HRas-induced OS cells upregulated degranulation markers including CD18, CD11b and CD63, as well as the activation markers ICAM1 and PD-L1 compared to co-cultures with control HMEC (**Fig 4g**). All these results clearly highlight the specific recruitment and functional activation of neutrophils by cells undergoing OS.

Preneoplastic cells activate the UPR and are sensed by neutrophils *in vivo*

To validate the relevance of our observations in spontaneous breast cancer models, we used 2 murine models of mammary tumorigenesis for which we have access to data from preneoplastic stage (closest *in vivo* equivalent of the *in vitro* OS stage). The first mouse model is a spontaneous breast cancer model that selectively expresses the *Neu*/ERBB2/HER2 oncogene in epithelial cells under the control of the MMTV (Mouse Mammary Tumor Virus) promoter. The preneoplastic stage (hyperplasia with dysplasia) was identified by histopathological analyses of mammary glands (between 6 and 8 weeks of age) (**Fig 5a**), and bulk RNA sequencing on sorted mammary epithelial cells ($CD45^-$ $EpCAM^+$) was performed. We validated the overexpression of the oncogene (**Fig S5a**) and its signature (**Fig 5b**) in Neu^+ mice compared to control mice (Neu^-). Consistently with our *in vitro* observations in human HRas-induced OS cells, preneoplastic epithelial cells showed an enrichment in an ER stress response signature (**Fig 5c**) and overexpressed the chemoattractant CXCL1 suggesting their potential to recruit neutrophils (**Fig 5d**). Through immunofluorescence staining using the Ly6G marker on FFPE tissues we revealed the strong recruitment of neutrophils at the preneoplastic stage, with 4-fold increase compared to healthy tissue

(**Fig 5e**). Second, we used publicly available scRNA-seq data from a mouse model BLG-cre; BRCA1$^{f/f}$; p53$^{+/-}$ of triple negative breast cancer (TNBC) arising from luminal progenitor cells[44]. Based on their prior analyses, we conducted pseudo-bulk analyses on isolated luminal progenitor cells from wild-type (WT) tissue and pre-cancerous stages. Principal component analysis revealed 3 distinct groups of luminal progenitor cells: a WT-like group closely resembling WT luminal progenitors, and 2 additional pre-cancerous groups, designated as stage I and II (**Fig 5f**). Interestingly, ssGSEA analysis reveals increase of the UPR signature scores starting at stage I, with a pronounced amplification observed at stage II (**Fig 5g**). We established this mouse model in our lab and identified the preneoplastic stage, encompassing stage I and stage II from previous results, to analyze neutrophil infiltration. Our analysis revealed that preneoplastic tissues exhibit increased immune cell recruitment (**Fig S5b**), with a particular enrichment of neutrophils among the immune cell populations (**Fig 5h**). Altogether, these results are consistent with the results obtained *in vitro* with HRas-induced OS cells, and demonstrate the crucial role of neutrophils in the early detection of cells undergoing UPR-mediated OS *in vivo*.

DISCUSSION

Understanding the intrinsic and extrinsic immunosurveillance mechanisms that occur during the early stages of OS is essential for identifying original signaling pathways that may be bypassed in established tumors or senescence contexts. These insights have the potential to reveal new therapeutic targets. The current study demonstrates that non-transformed human mammary epithelial cells adapt to OS by activating the UPR *in vitro*, which regulates key elements of their immunogenic profile encompassing an immunoactive secretome (SOS) and membrane ligands, thereby fostering an environment conducive to the activation and recruitment of neutrophils. We validated the intrinsic activation of the UPR in epithelial cells and the recruitment of neutrophils at preneopastic stage in 2 spontaneous breast cancer mouse models.

In this study, we established an innovative *in vitro* model of non-transformed human mammary epithelial cells (HMEC) undergoing OS, which progresses into oncogene-induced senescence (OIS). While the senescence-associated secretory phenotype (SASP) and its immunogenic properties have been well-characterized[4,45,46] (**www.SASPAtlas.com**) and validated in our model (**Fig. S1g-h**), we identified that cells experiencing OS produce an earlier secretome, termed Secretome of Oncogenic Stress (SOS) (**Fig. 1g-j**). This observation aligns with previous studies showing that stressed mouse embryonic

fibroblasts (MEFs) and KRas^{G12V} hepatocytes overexpressing p21, a key regulator of the DDR[47], release a distinct secretome preceding the SASP, referred to as the p21-activated secretory phenotype (PASP)[10]. However, HMEC undergoing OS activate the adaptive unfolded protein response (UPR) (**Fig. 2a; Fig. 5c, g**), through the IRE1 and PERK pathways (**Fig. 2b-e**), while the DDR remains inactive (**Fig. S1d, f**). Unlike the PASP, the SOS and, more specifically, the secretion of IL-8, GM-CSF and CXCL1 are regulated in an IRE1-dependent manner (**Fig. 3c**), as it has been described in MDA-MB-231 triple-negative breast cancer cell line[48]. Our findings raise intriguing questions about the preferential activation of specific adaptive intrinsic pathways, such as the UPR or DDR, depending on the cell type, the tissue origin and the driver oncogene. It would be valuable to investigate, for example, whether HRas^{G12V} overexpression in MEFs activates p21 or the UPR and how these different adaptive intrinsic pathways contribute to the composition of the secretome.

In addition to secreted factors, HMEC undergoing OS cells express immunogenic membrane ligands, including ULBP2-5-6, ICAM1, and PD-L1 (**Fig. 1e, k**). The early expression of PD-L1 is particularly intriguing, as it is classically associated with senescent cells[49,50] and cancer cells[51], where it facilitates immune evasion by inhibiting cytotoxic T cells[17,52] and NK cells[53] through its interaction with PD-1. Its presence at OS stage suggests that mechanisms of immune escape may be initiated far earlier in tumorigenesis than previously thought, particularly in Ras-driven oncogenesis, and highlights the potential efficacy of Immune Checkpoint Inhibitors (ICIs) in preneoplastic stages to intercept disease progression. We provide further insights into PD-L1 regulation by showing that HRas-driven OS upregulates PD-L1 expression independently of UPR pathways (**Fig 3e**), whereas in macrophages, PD-L1 upregulation relies on IRE1 activity[54]. This UPR-independent regulation could be explained by a previous study demonstrating that activation of the Ras pathway stabilizes PD-L1 mRNA, leading to its overexpression[31]. It would nonetheless be interesting to investigate the regulation of PD-L1 by UPR pathways, which appears to differ depending on the context and cell type.

Interestingly, similar to their role at sites of infection or tissue damage, neutrophils are the primary immune cells recruited to OS sites. Indeed, we demonstrated *in vitro* that they are the only immune cell population (**Fig 4a-b, S4a)** capable of being chemoattracted by the SOS, including IL-8 being the most potent attractor of neutrophils in humans[55]. We then showed that neutrophil levels increase at preneoplastic stages *in vivo* (**Fig 5e, h**), likely driven by CXCL1 expression (**Fig 5e**), which has already been reported to cause neutrophil accumulation by senescent endothelial cells[56]. These findings

highlight neutrophils as key immune players in the detection of stressed cells and complement existing knowledge that initially emphasizes the unique role of NK cells in this function[57].

Once recruited, neutrophils are activated under OS conditions (**Fig 4e-g**), and we may hypothezise that they play a pivotal role in the elimination of OS cells. First, neutrophils could eliminate OS cells through an antibody-dependent cellular cytotoxicity (ADCC) mechanism, known as trogoptosis, which is dependent on the Mac-1/integrins axis, mediating the formation of a cytotoxic synapse[58]. This is supported by our observation that ICAM1 is overexpressed on OS cells (**Fig 1k**), while activated neutrophils upregulate CD18 and CD11b (**Fig 4g**). Second, neutrophils may recruit other immune cells to kill OS cells, notably NK cells through the secretion of various chemokines, including CCL2, CCL3, and CCL4[59]. NK cells emerge as an interesting immune population, given our observation that OS cells overexpress NKG2D ligand family members (**Fig 1e**) and ICAM1 (**Fig 1k**), that are both described to drive senescent[28] and tumor[60] cells elimination by NK cells.

MATERIALS AND METHODS

Lead contact

Further information and requests for ressources and reagents should be directed to and will be fulfilled by the lead contact, Marie-Cécile Michallet (Marie-Cecile.MICHALLET@lyon.unicancer.fr)

MATERIALS AVAILABILITY

All reagents used in this study are summarized in Table S2-S7.

All reagents generated in this study are available upon reasonable request to the lead contact.

Data and code availability

- The Microarray data is available at : XXX RNAseq data is available at : XXX
- Any additional information required to reanalyze the data reported in this paper is available from the lead contact upon request

METHODS

Mouse tumor models and experiments

MMTV-Neu mouse model

MMTV-NeuT transgenic mice were provided by Dr. Virginie Petrilli and bred under specific pathogen-free (SPF) conditions at the Small animal core facility/imaging platform (P-PAC platform, CRCL, Lyon, France). Neu+/- BALB/c males were crossed with wild-type BALB/c females (Charles River Laboratories). As described in the literature, the early stage of tumor development, characterized by atypical mammary hyperplasia, occurs between the 5th and 13th weeks in mice expressing the Neu oncogene[61]. We validated this early stage by analyzing organs that were formalin-fixed, paraffin-embedded, and processed for hematoxylin and eosin staining (Research pathology platform East (PAR), CRCL, Lyon, France). The pathological examination of the slides was performed by Dr. Sara Belluco, a veterinary pathologist from VetAgro Sup (Ecole Vétérinaire Nationale, Lyon, France). Experiments were approved by the local and the French Ethical Committee for Animal Experimentation (#30253).

BLG-Cre, BRCA1$^{f/f}$, p53$^{+/-}$ mouse model

Cre recombinase expression is driven by the β-lactoglobulin (BLG) promoter, and exons 22-24 of BRCA1 are floxed, while one allele of Trp53 is mutated[62]. To initiate tumorigenesis through conditional BRCA1 deletion in the secretory epithelial cells of mammary glands, female BLG-Cre, BRCA1$^{f/f}$, p53$^{+/-}$ mice were mated with male BRCA1$^{f/f}$, p53$^{+/-}$ mice. To ensure 100% penetrance, female mice underwent two cycles of gestation and lactation, developing spontaneous and sporadic mammary tumors 18 to 56 weeks after Cre activation, with a median onset at 36 weeks. For control mice, female BRCA1$^{f/f}$, p53$^{+/+}$ mice were mated with male BLG-Cre, BRCA1$^{f/f}$, p53$^{+/-}$ mice and also underwent two cycles of gestation and lactation to maintain comparable physiological conditions. At 36 weeks post-first mating, tumor-free mammary glands from female BLG-Cre, BRCA1$^{f/f}$, p53$^{+/-}$ mice (representing the early stage of tumor development) and healthy mammary glands from control mice were harvested, and cell suspensions were prepared for staining with a specific surface marker panel (**Table S2a**). Experiments were approved by the local and the French Ethical Committee for Animal Experimentation (#38957).

Generation of cell suspensions from murine mammary tissues

Mice were euthanized by cervical dislocation, and mammary tissues were collected, weighed, minced, and digested with 1mg/mL Collagenase IA and 0,02mg/mL DNase (Sigma, ref#C2674 and ref#D4513) for 30’ at 37°C. The digested tissues were filtered on 70µm and 30µm cell strainers, centrifuged (300g, 10’, 10°C). Cells were resuspended in RPMI 1640 (Gibco, ref#72400-021) supplemented with 100U/mL of penicillin and 100µg/mL of streptomycin (Gibco, ref#15140-122) and 10% FBS (Eurobio, ref#CVFSVF00-01) for further experiments.

Cell Sorting of Epithelial Cells

For immunofluorescent staining, cells were incubated with FcBlock (Purified, Biolegend, ref#101301) for 15’ at 4°C in the dark, followed by staining with a mix of fluorescent-conjugated antibodies (**Table S2b**)

to identify epithelial cells, incubating for 30' at 4°C in the dark. Cells were washed twice with FACS buffer (PBS1x + 2mM EDTA, 3% FBS). After the final centrifugation (5', 1500rpm, 4°C), cells were resuspended and filtered in a 1x DAPI solution diluted in Pre-Sort FACS buffer (BD, ref#563503) at a concentration of 15.10^6 cells/ml. Epithelial cells (5000 cells) were sorted by flow cytometry (BD FACS Aria™ II) into 300µl of TCL lysis buffer (Qiagen, ref#1031576) supplemented with 1% β-mercaptoethanol (Sigma, ref#M6250). Tubes were vortexed briefly, immediately snap-frozen in liquid nitrogen, and stored at -80°C.

Library Preparation and RNA-Sequencing

Total RNA was extracted using the Single Cell RNA Purification Kit (Norgen, ref#51800), according to manufacturer's instructions, with an additional RNAse-free DNAse treatment (Qiagen, ref#79254). RNA quality (RNQ and DV200) was assessed using the Ultra Sentivity RNA Kit (Agilent, ref#FP-1201-0275) and the FemtoPulse system (Agilent) at the Gentyane Platform (Clermont-Ferrand, France). Following to manufacturer's instructions, libraries were prepared with the SMART-Seq Stranded Mammalian Single Cell Kit (Takara/Clontech, ref#634442) and sequenced on a NovaSeq Illumina platform (Cancer Genomics Platform, CRCL, Lyon, France) with a paired-end mode and a targeted depth of 32M reads/sample.

RNAseq data processing

For careful quality controls, raw data were aligned on the human genome (GRCh38) with STAR (v2.7.8a)[63], with the annotation of known genes from gencode v37. RNA quality controls metrics were computed using RSeQC (v4.0.0)[64]. Gene expression was quantified with Salmon (v1.5)[65] on the raw sequencing reads, using the annotation from gencode v38 as index. Single sample GSEA (ssGSEA) scores were computed on TPM normalized data through gsva R package (v1.50.0)[66] using mouse pathways annotations from msigdb R package (v.1.10.0)[67,68] (**Table S3a**).

Multiplex Immunofluorescence (mIF)

Murine mammary glands were collected directly into 4% formaldehyde and embedded in paraffin. Serial sections were cut into 4µm slices using a microtome (PAR Platform). Multiplex immunofluorescence (mIF) staining (4-color) was performed on a slide using the Leica BOND RX automated system. Slides were stained with antibodies (**Table S4**) based on the OPAL system (Akoya Biosciences). Nuclei were counterstained with DAPI (Akoya Biosciences). Slides were then digitized at 20x magnification using the Vectra Polaris multispectral scanner (Akoya Biosciences) and visualized with the Phenochart viewer (Akoya Biosciences).

Analysis of Publicly scRNA-seq dataset from BRCA1-mutated mammary tumor model

Publicly available scRNA-seq dataset from the BRCA1-mutated mouse mammary tumor model (BLG-CRE, $BRCA^{f/f}$, $p53^{+/-}$)[44] was utilized to characterized ER stress and UPR response on epithelial cells during tumor progression. In this study, the authors sorted live cells from mammary glands at different stages during tumor development and performed scRNA-seq using 10X Genomics technology. Dataset processing and analyses were performed using Seurat (version 5.0). After normalization (LogNormalize)

and scaling, principal component analysis (PCA) was performed on non-tumor epithelial cells following a pseudo-bulk approach, where gene expression of individual cells within each sample was aggregated. Based on the PCA results, samples were stratified into 3 pre-cancer stages: WT-like, Stage-I and Stage-II. Gene signature scores of ER stress and UPR pathways from REACTOME, HALLMARKS and Gene Ontology (GO) databases (**Table S3a**), were calculated for each cell using Ucell package (version 2.10.1) and the *AddModuleScore_UCell* function of Seurat.

Human models and experiments

Human Mammary Epithelial Cell Line Generation

Human mammary epithelial cells (HMEC - Promocell, ref#C-12650) were immortalized with by transduction with a retroviral vector pBABE-puro containing the Human Telomerase Reverse Transcriptase (hTERT - Addgene). HMEC-hTERT cells then transduced with a lentiviral plasmid/vector pLVUT' for doxycycline-inducible HRas^{G12V} (HMEC-HRas) of Green Fluorescence Protein (HMEC-GFP) expression (tet ON system - Trono/Aebischer's lab). Cells were cultured in Mammary Epithelium Cell Growth Medium (MECGm – Promocell, ref#CC-5012) supplemented with 100U/mL of penicillin and 100µg/mL of streptomycin (Gibco, ref#15140-122). Upon reaching 75% confluence, cells were washed with PBS1x (Gibco, ref#11540486), trypsinized with Trypsin/EDTA (0.25 mg/mL - Lonza, ref#CC-5012) for 20' at 37°C, and neutralized with Trypsin Neutralizing Solution (TNS - Lonza, ref#CC-5002). Cell suspension was centrifuged (5', 1400rpm, room temperature (RT)), and the pellet was re-suspended in 37°C MECGm before plating.

In vitro HRas^{G12V} and GFP Induction Assay

At day -1 (d-1), cells were plated at 1% of confluency in culture dishes or culture plates. At d0, culture medium was replaced by MECGm supplemented or not with doxycycline (1µg/mL – Sigma, ref#D9891-1G) in order to induce or not HRas^{G12V} or GFP. Supplemented mediums were then daily refreshed.

Human Immune cells Isolation

Immune cells were isolated from healthy donor blood samples of the "Etablissement Français du Sang" (Lyon) according manufacturer's instruction. Briefly, to obtain total immune cells, blood was lysed with 1x lysing buffer (4,5mL of blood for 45mL of lysing buffer, BD Pharm Lyse – BD, ref#555899). To isolate peripheral blood mononuclear cells (PBMCs), the standard Ficoll method (Eurobio, ref#CMSMSL01-01) was used. For neutrophil isolation, the EasySep™ Direct Human Neutrophil Isolation Kit (Stemcell, ref#19666) was employed.

Morphology Assessment

Cells were imaged daily using an Axiovert25 microscope (Zeiss) with 20x magnification and analyzed using Zen software.

SA-β-galactosidase Activity

β-galactosidase staining was performed using the Cell Signaling β-galactosidase staining kit (Cell signaling, ref#9860). Cells were fixed and stained with X-Gal substrate (1mg/mL, pH6) overnight at 37°C in a dry incubator.

Microarray Analyses

Microarrays analyses were performed to identify differentially expressed genes/pathways between d3 (OS of kinetics - n=4) and d5 (OIS of kinetics - n=3) and their control. Briefly, at d3 or d5 of the kinetics, supernatants were removed, and cells were washed with PBS1x. Then, cells were lysed directly in plate, in 350µl of RLT buffer (Qiagen, ref#79216). Lysates were vortexed, snap frozen and conserved at –80°C. RNA extraction, reverse transcription and microarray hybridization on Affymetrix GeneChip Human PrimeView arrays (Affymetrix). Microarray data analysis was conducted in R (version 4.3.3). Raw probe intensities were quantile normalized and log2-transformed using the Robust Multi-array Averaging (RMA) method available in the affy package (v. 1.80.0). We identified Differentially expressed genes (DEG) between OS cells and their control by using DESeq2 (v. 1.42.1) with an adjusted p-value (adj.P.Val) < 0.05 and a log2 fold change > 0.58. Their locations were determined by using the database Uniprot (**https://www.uniprot.org/**). Single sample Gene set enrichment analyses (ssGSEA) were performed by using the GSVA package (v. 1.50.5) and the Molecular Signatures Database into Human collection (Human MSigDB v2024.1.Hs). Used genesets are presented in **Table S3b**. The statistical significance of ssGSEA score was addressed with two-tailed Wilcoxon test, with α=0,05.

Immunoblotting

HMEC-HRas were lysed on ice in Laemmli 2x buffer (0.125M Tris HCl pH 6.8 (Euromedex, ref#EU0011; Fisher, ref#H/1150/PB15), 2% SDS (Euromedex, ref#EU0460), 0.5M DTT (Euromedex, ref#EU0006-D)). Protein quantification was performed using Bradford reagent (Bio-Rad, ref#5000006) with Bovine Serum Albumin standards (Sigma, ref#A9647). For each condition, 20µg of denatured protein was resolved on 8 or 12% SDS-PAGE and transferred to nitrocellulose membranes using the Trans-Blot® Turbo Transfer System (Bio-Rad, ref#17001918). Membranes were blocked in TBS-Tween 5% BSA, probed with primary antibodies (**Table S5**) overnight at 4°C, washed, and incubated with HRP-conjugated secondary antibodies. Signals were detected using Clarity™ Western ECL substrate (Bio-Rad, ref#170-5061) and the ChemiDoc Imaging System (Bio-Rad). Results were analyzed with Image Lab software (Bio-Rad).

RNA Extraction and RT-qPCR

Total RNA was extracted using the Nucleospin RNA kit (Macherey Nagel, ref#740955) according to the manufacturer's instructions. RNA was quantified by NanoDrop™ One (Thermo Scientific), and retrotranscription of 1000ng of RNA was performed using the iScript kit (Bio-Rad, ref#1725038). qPCR was carried out using a CFX Connect™ Real-Time System (Bio-Rad) with SYBR Green (Bio-Rad, ref#1725271) and 10µM primers (**Table S6**) for a total of 40 cycles, as follows: 95°C for 15sec, 60°C for 20sec, and 95°C for 15sec. Results were represented as mean ratio of the gene of interest on the housekeeping gene (GUS), and normalize as fold of the corresponding "control" sample

ELISA

ELISA kits (**Table S7**) were used according to the manufacturer's instructions. Briefly, ELISA plates (Nunc Maxisorp - Thermo Scientific, ref#442404) were coated with capture antibodies, blocked with PBS1X - 1% BSA, and incubated with cell line supernatants, standards, or controls in duplicates. After washing, HRP-conjugated detection antibodies were added, and 3,3',5,5'-tetramethylbenzidine (TMB) enzymatic substrate (Interchim, ref#UP664781) was used for signal development. Optical density was read at 450nm with correction at 540–570nm using a Multiskan FC reader (Thermo Scientific).

Transwell Migration Assay

After isolation, immune cells pellets were resuspended in MECGm at 5×10^6 cells/mL. In Transwell plates, 600µL of conditioned media was added and 100µL of neutrophils suspension was added to inserts with a porosity of 3µm (Corning, ref#003415) and total immune cells or PBMCs was added to inserts with a porosity of 5µm (Corning, ref#003421), in duplicate. Cells migrated for 3h at 37°C, 5% CO_2. Immune cells were stained with a specific surface marker panel (**Table S2c-d**) and 20µL of Flow Count beads (Beckman Coulter, ref#7547053) were added before analysis.

p-STAT5 Activation

Total immune cells were resuspended in 1mL of conditioned medium (normalized to cell culture number) to achieve 2×10^6 immune cells/mL. Neutrophils were incubated for 30' at 37°C, 5% CO_2, centrifuged (5', 1500rpm, 37°C) and stained with specific surface marker panel (**Table S2e**).

ROS Production

Isolated neutrophils were resuspended in 1mL of conditioned supernatants (normalized to cell culture number) at $0{,}5\times10^6$ neutrophils/mL and incubated for 12h at 37°C, 5% CO_2. Neutrophils were transferred to a 96-well V-bottom plate on ice, washed with PBS1x, and stained with Zombie NIR for viability. After two washes with FACS buffer (PBS1x + 2 mM EDTA, 3% FBS), pellets were resuspended in 100µL of ROS-detection solution (CM-H2DCFDA - Invitrogen, ref# C6827) and incubated for 20' at RT, protected from light. Cells were washed and stained with a specific surface marker panel (**Table S2f**).

Co-culture Assay

At d2,5 cells were co-cultured with isolated neutrophils at a at a ratio of 1 HMEC to 5 neutrophils for 12h. After co-culture, cells were harvested, centrifuged (5', 1500rpm, RT) and stained with a specific surface marker panel (**Table S2g**) to assess neutrophil activation and degranulation.

***In Vitro* Matrigel Assay**

At d0, HMEC were resuspended in cold MECGm at $0{,}5\times10^6$ cells/mL. A 100µL cell suspension was mixed with 500µl Matrigel growth factor reduced (Corning, ref#354230), with or without dox (1,7µg/mL), on ice. The mixture was gently agitated, incubated on ice for 1h, then drawn into a cold syringe and layered in a 12w plate. Plates were incubated at 37°C with 5% CO_2 for 45', followed by the addition of 1mL MECGm with or without dox (1µg/mL). Media were refreshed daily.

At d3 or d5, supernatants were collected and matrigel with cells were recovered with 2mL cold MECGm, transferred to a 50mL tube, diluted with 28mL cold MECGm, and centrifuged twice (5‘, 1500 rpm, 4°C). Cells were treated with 10mL Trypsin-EDTA 0.05% (Gibco, ref#25300-054) for 20’ at 37°C with 5% CO_2, followed by neutralization with 10mL MECGm. After centrifugation (5’, 1500rpm, RT), cells were counted and snap-frozen.

***In Vivo* Matrigel Plug Assay**

Experiments were performed on female NMRI Nude mice (Charles River). A total of 50 000 cells were suspended in 100µl PBS1x and mixed with 400µL Matrigel growth factor reduced (Corning, ref#354230). The mixture was injected subcutaneously into the back of mice under isoflurane anesthesia. After three days, mice were sacrificed, and Matrigel plugs were collected. Infiltrating cells were isolated by enzymatic dissociation using Dispase (Corning, ref#354235), Collagenase A (Roche, ref#10103586001), and DNAse I (Roche, ref#05952077103) for 30’ at 37°C and were stained with a specific surface marker panel (**Table S2h**).

Flow Cytometry

Extracellular Staining

Cell suspensions were plated in a 96-well V-bottom plate, centrifuged (5’ at 1400rpm, RT), and resuspended in 100µL to assess viability. After a 25’ incubation at 4°C in the dark, cells were washed twice with FACS buffer (PBS1x + 2 mM EDTA, 3% FBS) and incubated for 25’ at 4°C with a mix of a specific surface marker panel antibodies (**Table S2**). Following two washes with FACS buffer, cells were fixed with 4% formaldehyde (Sigma, ref#F8775-500ML) for 20’ at 4°C. Cells were resuspended in 200µL of FACS buffer, transferred to Micronic tubes. Samples were analyzed on LSRFortessa™ (BD Biosciences) or Cytek® Aurora (Cytek Biosciences), and data were processed with FlowJo software.

Intracellular Staining

After extracellular staining, cells were washed with PBS1x and fixed in preheated BD Lyse/Fix Buffer (BD, ref# 558049) for 10 min at 37°C under 5% CO_2. After washing with PBS1X, cells were permeabilized with pre-chilled Perm Buffer III (BD, ref# 558050) for 30’ on ice in the dark. Following washes, intracellular antibodies (**Table S2**) diluted in FACS buffer were added, and cells were incubated for 45’ in the dark. After a final wash, cells were resuspended in 200µL of FACS buffer, transferred to Micronic tubes, and analyzed using LSRFortessa™ (BD Biosciences) and FlowJo software.

Statistical Analysis

All data analyses were performed using Prism Version 10.3.1 (GraphPad Software). The number of independent experiments is indicated in the legends of each figure. First, a Shapiro-Wilk normality test was performed on all data sets. Then according to these results parametric (normality) and nonparametric (does not follow the normal law) tests were used. The statistical significance of proliferation data was addressed with a Two-Way ANOVA test using Geisser-Greenhouse correction method, with α=0,05 (*$p<0.05$; **$p<0.01$, ***$p<0.001$; ****$p<0.0001$; non-significant results defined as $p\geq0.05$ had ns). The statistical significance of RT-qPCR, ELISA, immunogenic membrane ligands

staining, neutrophil migration and activation, matrigel assay and neutrophil infiltration in mouse models data was addressed with a two-tailed Wilcoxon test (*$p<0.05$; **$p<0.01$, ***$p<0.001$; ****$p<0.0001$; non-significant results defined as $p\geq0.05$ had ns). The statistical significance of microarray data was addressed with Mann-Whitney test or One-way ANOVA with $\alpha=0,05$ (*$p<0.05$; **$p<0.01$; ***$p<0.001$; ****$p<0.0001$, ns $p\geq0.05$). The statistical significance of RNAseq data of MMTV-Neu mouse model was addressed with Welch's t test with $\alpha=0,05$ (*$p<0.05$; **$p<0.01$; ***$p<0.001$; ****$p<0.0001$, ns $p\geq0.05$). The statistical significance of data with HMEC treated or not with UPR inhibitors (ELISA, immunogenic membrane ligands) was addressed with RM-one-Way ANOVA test using Geisser-Greenhouse correction method, with $\alpha=0,05$ (*$p<0.05$; **$p<0.01$; ***$p<0.001$; ****$p<0.0001$, ns $p\geq0.05$).

REFERENCES

1. Abbadie, C., Pluquet, O. & Pourtier, A. Epithelial cell senescence: an adaptive response to pre-carcinogenic stresses? *Cell. Mol. Life Sci.* **74**, 4471–4509 (2017).
2. Prieto, L. I., Sturmlechner, I., Goronzy, J. J. & Baker, D. J. Senescent cells as thermostats of anti-tumor immunity. *Sci. Transl. Med.* **15**, eadg7291 (2023).
3. Hernandez-Segura, A., Nehme, J. & Demaria, M. Hallmarks of Cellular Senescence. *Trends Cell Biol.* **28**, 436–453 (2018).
4. Coppé, J.-P. *et al.* Senescence-Associated Secretory Phenotypes Reveal Cell-Nonautonomous Functions of Oncogenic RAS and the p53 Tumor Suppressor. *PLOS Biol.* **6**, e301 (2008).
5. Hernandez-Segura, A. *et al.* Unmasking Transcriptional Heterogeneity in Senescent Cells. *Curr. Biol.* **27**, 2652-2660.e4 (2017).
6. Basisty, N. *et al.* A proteomic atlas of senescence-associated secretomes for aging biomarker development. *PLoS Biol.* **18**, e3000599 (2020).
7. Krizhanovsky, V. *et al.* Senescence of activated stellate cells limits liver fibrosis. *Cell* **134**, 657–667 (2008).
8. Iannello, A., Thompson, T. W., Ardolino, M., Lowe, S. W. & Raulet, D. H. p53-dependent chemokine production by senescent tumor cells supports NKG2D-dependent tumor elimination by natural killer cells. *J. Exp. Med.* **210**, 2057–2069 (2013).
9. Xue, W. *et al.* Senescence and tumour clearance is triggered by p53 restoration in murine liver carcinomas. *Nature* **445**, 656–660 (2007).
10. Sturmlechner, I. *et al.* p21 produces a bioactive secretome that places stressed cells under immunosurveillance. *Science* **374**, eabb3420 (2021).
11. Gasser, S., Orsulic, S., Brown, E. J. & Raulet, D. H. The DNA damage pathway regulates innate immune system ligands for the NKG2D receptor. *Nature* **436**, 1186–1190 (2005).
12. Iannello, A. & Raulet, D. H. Immune Surveillance of Unhealthy Cells by Natural Killer cells. *Cold Spring Harb. Symp. Quant. Biol.* **78**, 249–257 (2013).
13. Petti, C. *et al.* Coexpression of NRASQ61R and BRAFV600E in Human Melanoma Cells Activates Senescence and Increases Susceptibility to Cell-Mediated Cytotoxicity. *Cancer Res.* **66**, 6503–6511 (2006).
14. van Tuyn, J. *et al.* Oncogene-Expressing Senescent Melanocytes Up-Regulate MHC Class II, a Candidate Melanoma Suppressor Function. *J. Invest. Dermatol.* **137**, 2197–2207 (2017).
15. Marin, I. *et al.* Cellular Senescence Is Immunogenic and Promotes Antitumor Immunity. *Cancer Discov.* **13**, 410–431 (2023).
16. Marin, I. *et al.* Cellular Senescence Is Immunogenic and Promotes Antitumor Immunity. *Cancer Discov.* **13**, 410–431 (2023).
17. Wang, T.-W. *et al.* Blocking PD-L1–PD-1 improves senescence surveillance and ageing phenotypes. *Nature* **611**, 358–364 (2022).
18. Chaib, S. *et al.* The efficacy of chemotherapy is limited by intratumoral senescent cells expressing PD-L2. *Nat. Cancer* 1–15 (2024) doi:10.1038/s43018-023-00712-x.
19. Pereira, B. I. *et al.* Senescent cells evade immune clearance via HLA-E-mediated NK and CD8+ T cell inhibition. *Nat. Commun.* **10**, 2387 (2019).
20. Iltis, C. *et al.* A ganglioside-based immune checkpoint enables senescent cells to evade immunosurveillance during aging. *Nat. Aging* 1–18 (2024) doi:10.1038/s43587-024-00776-z.
21. Łukasiewicz, S. *et al.* Breast Cancer—Epidemiology, Risk Factors, Classification, Prognostic Markers, and Current Treatment Strategies—An Updated Review. *Cancers* **13**, 4287 (2021).
22. Dvir, K., Giordano, S. & Leone, J. P. Immunotherapy in Breast Cancer. *Int. J. Mol. Sci.* **25**, 7517 (2024).
23. Feng, Y. *et al.* Breast cancer development and progression: Risk factors, cancer stem cells, signaling pathways, genomics, and molecular pathogenesis. *Genes Dis.* **5**, 77–106 (2018).
24. Collin, G., Huna, A., Warnier, M., Flaman, J.-M. & Bernard, D. Transcriptional repression of DNA repair genes is a hallmark and a cause of cellular senescence. *Cell Death Dis.* **9**, 259 (2018).
25. Saul, D. *et al.* A new gene set identifies senescent cells and predicts senescence-associated pathways across tissues. *Nat. Commun.* **13**, 4827 (2022).
26. Fridman, A. & Tainsky, M. Critical pathways in cellular senescence and immortalization revealed by gene expression profiling. *Oncogene* **27**, 10.1038/onc.2008.213 (2008).
27. Jones, A. B., Rocco, A., Lamb, L. S., Friedman, G. K. & Hjelmeland, A. B. Regulation of NKG2D Stress Ligands and Its Relevance in Cancer Progression. *Cancers* **14**, 2339 (2022).
28. Sagiv, A. *et al.* NKG2D ligands mediate immunosurveillance of senescent cells. *Aging* **8**, 328–344 (2016).

29. Frisch, S. M. & MacFawn, I. P. Type I interferons and related pathways in cell senescence. *Aging Cell* **19**, e13234 (2020).
30. Marin, I., Serrano, M. & Pietrocola, F. Recent insights into the crosstalk between senescent cells and CD8 T lymphocytes. *NPJ Aging* **9**, 8 (2023).
31. Coelho, M. A. *et al.* Oncogenic RAS Signaling Promotes Tumor Immunoresistance by Stabilizing PD-L1 mRNA. *Immunity* **47**, 1083-1099.e6 (2017).
32. Vanacker, H. *et al.* Emerging Role of the Unfolded Protein Response in Tumor Immunosurveillance. *Trends Cancer* **3**, 491–505 (2017).
33. Pluquet, O. & Abbadie, C. Chapter Seven - Cellular senescence and tumor promotion: Role of the Unfolded Protein Response. in *Advances in Cancer Research* (eds. Gewirtz, D. A. & Fisher, P. B.) vol. 150 285–334 (Academic Press, 2021).
34. Blazanin, N. *et al.* ER stress and distinct outputs of the IRE1α RNase control proliferation and senescence in response to oncogenic Ras. *Proc. Natl. Acad. Sci. U. S. A.* **114**, 9900–9905 (2017).
35. Denoyelle, C. *et al.* Anti-oncogenic role of the endoplasmic reticulum differentially activated by mutations in the MAPK pathway. *Nat. Cell Biol.* **8**, 1053–1063 (2006).
36. Kim, H. S. *et al.* The p38-activated ER stress-ATF6α axis mediates cellular senescence. *FASEB J.* **33**, 2422–2434 (2019).
37. Masuda, H. *et al.* Role of Epidermal Growth Factor Receptor in Breast Cancer. *Breast Cancer Res. Treat.* **136**, 10.1007/s10549-012-2289–9 (2012).
38. Sparta, B. *et al.* Receptor Level Mechanisms Are Required for Epidermal Growth Factor (EGF)-stimulated Extracellular Signal-regulated Kinase (ERK) Activity Pulses. *J. Biol. Chem.* **290**, 24784–24792 (2015).
39. Mukhopadhyay, S., Vander Heiden, M. G. & McCormick, F. The Metabolic Landscape of RAS-Driven Cancers from biology to therapy. *Nat. Cancer* **2**, 271–283 (2021).
40. Redding, A., Aplin, A. E. & Grabocka, E. RAS-mediated tumor stress adaptation and the targeting opportunities it presents. *Dis. Model. Mech.* **15**, dmm049280 (2022).
41. Huber, A.-L. *et al.* p58IPK-Mediated Attenuation of the Proapoptotic PERK-CHOP Pathway Allows Malignant Progression upon Low Glucose. *Mol. Cell* **49**, 1049–1059 (2013).
42. Hamanaka, R. B., Bennett, B. S., Cullinan, S. B. & Diehl, J. A. PERK and GCN2 Contribute to eIF2α Phosphorylation and Cell Cycle Arrest after Activation of the Unfolded Protein Response Pathway. *Mol. Biol. Cell* **16**, 5493–5501 (2005).
43. Pakos-Zebrucka, K. *et al.* The integrated stress response. *EMBO Rep.* **17**, 1374–1395 (2016).
44. Bach, K. *et al.* Time-resolved single-cell analysis of Brca1 associated mammary tumourigenesis reveals aberrant differentiation of luminal progenitors. *Nat. Commun.* **12**, 1502 (2021).
45. Catanzaro, J. M. *et al.* Oncogenic Ras induces inflammatory cytokine production by up-regulating the squamous cell carcinoma antigens SerpinB3/B4. *Nat. Commun.* **5**, 3729 (2014).
46. Hamarsheh, S., Groß, O., Brummer, T. & Zeiser, R. Immune modulatory effects of oncogenic KRAS in cancer. *Nat. Commun.* **11**, 5439 (2020).
47. Abbas, T. & Dutta, A. p21 in cancer: intricate networks and multiple activities. *Nat. Rev. Cancer* **9**, 400 (2009).
48. Logue, S. E. *et al.* Inhibition of IRE1 RNase activity modulates the tumor cell secretome and enhances response to chemotherapy. *Nat. Commun.* **9**, 3267 (2018).
49. Onorati, A. *et al.* Upregulation of PD-L1 in Senescence and Aging. *Mol. Cell. Biol.* **42**, e00171 (2022).
50. Majewska, J. *et al.* p16-dependent increase of PD-L1 stability regulates immunosurveillance of senescent cells. *Nat. Cell Biol.* **26**, 1336–1345 (2024).
51. Yi, M., Niu, M., Xu, L., Luo, S. & Wu, K. Regulation of PD-L1 expression in the tumor microenvironment. *J. Hematol. Oncol.J Hematol Oncol* **14**, 10 (2021).
52. Jiang, X. *et al.* Role of the tumor microenvironment in PD-L1/PD-1-mediated tumor immune escape. *Mol. Cancer* **18**, 10 (2019).
53. Niu, C. *et al.* PD-1-positive Natural Killer Cells have a weaker antitumor function than that of PD-1-negative Natural Killer Cells in Lung Cancer. *Int. J. Med. Sci.* **17**, 1964 (2020).
54. Batista, A. *et al.* IRE1α regulates macrophage polarization, PD-L1 expression, and tumor survival. *PLoS Biol.* **18**, e3000687 (2020).
55. Cambier, S., Gouwy, M. & Proost, P. The chemokines CXCL8 and CXCL12: molecular and functional properties, role in disease and efforts towards pharmacological intervention. *Cell. Mol. Immunol.* **20**, 217–251 (2023).
56. Rolas, L. *et al.* Senescent endothelial cells promote pathogenic neutrophil trafficking in inflamed tissues. *EMBO Rep.* 1–28 (2024) doi:10.1038/s44319-024-00182-x.

57. Raulet, D. H. & Guerra, N. Oncogenic stress sensed by the immune system: role of NK cell receptors. *Nat. Rev. Immunol.* **9**, 568–580 (2009).
58. Matlung, H. L. *et al.* Neutrophils Kill Antibody-Opsonized Cancer Cells by Trogoptosis. *Cell Rep.* **23**, 3946-3959.e6 (2018).
59. Tecchio, C. & Cassatella, M. A. Neutrophil-derived chemokines on the road to immunity. *Semin. Immunol.* **28**, 119–128 (2016).
60. Guia, S. *et al.* Genome-wide CRISPR/Cas9 screen reveals factors that influence the susceptibility of tumor cells to NK cell-mediated killing. 2024.10.08.615667 Preprint at https://doi.org/10.1101/2024.10.08.615667 (2024).
61. Boggio, K. *et al.* Interleukin 12–mediated Prevention of Spontaneous Mammary Adenocarcinomas in Two Lines of Her-2/neu Transgenic Mice. *J. Exp. Med.* **188**, 589–596 (1998).
62. McCarthy, A. *et al.* A mouse model of basal-like breast carcinoma with metaplastic elements. *J. Pathol.* **211**, 389–398 (2007).
63. Dobin, A. *et al.* STAR: ultrafast universal RNA-seq aligner. *Bioinformatics* **29**, 15–21 (2013).
64. Wang, L., Wang, S. & Li, W. RSeQC: quality control of RNA-seq experiments. *Bioinformatics* **28**, 2184–2185 (2012).
65. Patro, R., Duggal, G., Love, M. I., Irizarry, R. A. & Kingsford, C. Salmon: fast and bias-aware quantification of transcript expression using dual-phase inference. *Nat. Methods* **14**, 417–419 (2017).
66. Hänzelmann, S., Castelo, R. & Guinney, J. GSVA: gene set variation analysis for microarray and RNA-Seq data. *BMC Bioinformatics* **14**, 7 (2013).
67. Subramanian, A. *et al.* Gene set enrichment analysis: A knowledge-based approach for interpreting genome-wide expression profiles. *Proc. Natl. Acad. Sci.* **102**, 15545–15550 (2005).
68. Castanza, A. S. *et al.* Extending support for mouse data in the Molecular Signatures Database (MSigDB). *Nat. Methods* **20**, 1619–1620 (2023).
69. Guglietta, S. *et al.* Coagulation induced by C3aR-dependent NETosis drives protumorigenic neutrophils during small intestinal tumorigenesis. *Nat. Commun.* **7**, 11037 (2016).

Author Contributions

M.M., N.G. and L.M. developed the *in vitro* model; A.D, L.L., H.V., E.J., M.L., L.M., N.B.V. and M.C.M. designed the *in vitro* experiments; A.D, L.L., H.V., E.J., M.L. and L.M. performed *in vitro* experiments; J.C.V., I.M., A.D., L.M. and M.C.M. designed the matrigel experiments; J.C.V, I.M. and A.D. performed matrigel experiments; A.V. performed flow cytometry on BLG-cre; BRCA1$^{f/f}$; p53$^{+/-}$ and analyzed scRNAseq public data; M.P.A and M.C.M. performed RNAseq experiments on MMTV-Neu model; A.V., M.P.A., S.B. and C.A. performed *in situ* experiments and analyses; A.D., M.H., A.V. and R.P. performed bio-informatic analyses; A.D., L.M. and M.C.M. wrote the manuscript; A.D. and M.C.M. designed the figures and supplementary data; V.P., N.B.V. and C.C. provided input all along the study and on the manuscript. M.C.M. conceptualized and directed the study.

Conflict of interest

All authors declare that they have no competing interests.

Funding

A.D. was supported by grants from la Ligue Contre le Cancer PhD Grant 2021-2024 IP/SC/SK - 17250. We also want to thank the Plan Cancer (INCa-ITMO Cancer, Cancer PNP 2021), Ligue nationale labellisation équipe (EL2020-FNCLCC/chC), LYRICAN (INCa-DGOS-Inserm_12563), the Ruban Rose association, the BMS foundation, the Institut Convergence PLAsCAN (ANR-17-CONV-0002), the LABEX DEVweCAN (ANR-10-LABX-0061) of the University of Lyon and the RHU MyPROBE (ANR-17-RHUS-0008), both within the program Investissements d'Avenir organized by the French National Research Agency (ANR), and the LYRICAN (grant INCa-DGOS-Inserm_12563).

Acknowledgments

We thank technological platforms of the CRCL especially Thibault Andrieu, operational director of the Flow cytometry core facility (CYLE), Research pathology platform East (PAR), Small animal core facility/imaging platform (P-PAC), Cancer genomics platform (CGP) and "Gilles Thomas" bioinformatics platform (GILLES THOMAS PLATFORM). We also thank Julien Cherfils-Vicini team at the IRCAN for its invaluable support. Our sincere thanks go to the Etablissement Français du Sang (France) for supplying the blood samples.

FIGURE LEGENDS

Figure 1: Oncogenic Stress induces the expression of immunogenic secretome and membrane ligands

a. Scheme of the kinetic induction of oncogenic stress (OS) and oncogene-induced senescence (OIS) in HMEC-HRas model. Upon doxycycline-inducible $HRas^{G12V}$ expression, there is the OS stage at day 3 followed by the OIS phase at day 5.

b. Representative western blot analysis of Ras and its downstream factor ERK using whole cell lysates from a time-course experiment in untreated (Ctl at d3 and Ctl OIS at d5) and treated (OS at d3 and OIS at d5) HMEC-HRas.

c., d. Violin plots representing ssGSEA enrichment score of the HRas Oncogenic (**c.**) or Response to Stress (**d.**) signatures in Ctl and OS (n=4) or Ctl OIS and OIS (n=3) HMEC.

e. Representative histogram plot of ULBP2-5-6 expression monitored by flow cytometry in Ctl and OS HMEC (left panel). Box plot illustrating the median of fluorescence intensity (MFI) of the stress ligands expression (right panel) (n=10).

f. Pie chart representing the subcellular localization of differential expressed protein-coding genes from the comparison of OS versus Ctl HMEC.

g. Top 10 of secreted protein-coding genes among DEGs between OS and Ctl cells.

h. Quantification by ELISA of cytokines and chemokines production in Ctl and OS HMEC supernatants. Concentrations were normalized for 10^6 cells (n=6 to 13).

i. Violin plot representing ssGSEA enrichment score of the Response to type I Interferon in Ctl and OS HMEC (n=4).

j. Interferon-stimulated genes (ISG) expression were measured by RT-qPCR and normalized on Ctl HMEC (n=5 to 12).

k. Representative histograms and box plots showing the MFI of ICAM1 (left panel) and PD-L1 (right panel) in Ctl and OS HMEC (n=10).

Data information: (**c-d**) One-Way ANOVA test (***p<0.001; ****p<0.0001). (**e, h, j-k**) Two-tailed Wilcoxon test. Shown is the median ± SEM (*p<0.05; **p<0.01; ***p<0.001). (**i**) Mann-Whitney test (*p<0.05).

Figure 2: Oncogenic $HRas^{G12V}$ in HMEC triggers Endoplasmic Reticulum stress

a., b. Violin plots representing ssGSEA enrichment score of the ER stress Response (**a.**) or the IRE1 (left panel), PERK (central panel) and ATF6 (right panel) pathways (**b.**) signatures in Ctl and OS HMEC (n=4).

c. Representative western blot analysis of Unfolded Protein Response (UPR) sensors (IRE1, PERK and ATF6) and eiF2α phosphorylation (downstream of PERK) using whole cell lysates from Ctl and OS HMEC.

d., e. Box plots representing IRE1 (**d.**) and PERK (**e.**) target genes expression measured by RT-qPCR and normalized on Ctl HMEC.

Data information: (**a-b**) Mann-Whitney test (*p<0.05; ns p≥0.05). (**d-e**) Two-tailed Wilcoxon test. Shown is the median ± SEM (*p<0.05; ***p<0.001; ****p<0.0001).

Figure 3: Inhibition of PERK and IRE1 pathways affect the OS-induced immunogenicity

a. Scheme representing the protocol for pharmacological inhibition of the PERK (GSK-2606414) and IRE1 (4µ8c) pathways.

b., c. Quantification by ELISA of IL8, CXCL1, and GM-CSF production in Ctl and OS HMEC supernatants with or without PERK inhibition (**b.**) or IRE1 inhibition (**c.**). Concentrations were normalized by 10^6 cells.

d., e. Expression of ICAM1, ULBP2-5-6, and PD-L1 in Ctl and OS HMEC with or without PERK inhibition (**d.**) or IRE1 inhibition (**e.**) assessed by flow cytometry.

Data information: (**b-e**) RM one-Way ANOVA test. Shown is the mean ± SEM. (*p<0.05; **p<0.01; ***p<0.001; ****p<0.0001; ns p≥0.05).

Figure 4: Immunogenic potential of the OS is sensed by neutrophils

a., b. Schematic representation of transwell assays performed with total immune cells (**a.**) or isolated neutrophils (**b.**) (left panels). Box plots showing the recruitment of immune cell populations (**a.**, n=14) or neutrophils (**b.**, n=18) by Ctl or OS HMEC normalized supernatants monitored by flow cytometry (right panels).

c. Scheme of the matrigel assay *in vivo*: HMEC were embedded in matrigel without (Ctl) or with dox (OS) and then implanted into nude mice. After 3 days, the matrigel implants were recovered and neutrophils were identified by flow cytometry.

d. Box plots representing the frequency (left panel) or the number (right panel) of neutrophils among immune cells in matrigel containing Ctl or OS HMEC, assessed by flow cytometry (n=7).

e. Schematic representation of the p-STAT5 assay using total immune cells stimulated with normalized supernatants from Ctl or OS HMEC (left panel). Box plot showing the MFI of p-STAT5 in neutrophils, as measured by flow cytometry (right panel) (n=14).

f. Schematic representation of the reactive oxygen species (ROS) production assay using isolated neutrophils stimulated with normalized supernatants from Ctl or OS HMEC (left panel). Box plot showing the MFI of ROS in neutrophils, as measured by flow cytometry (right panel) (n=13).

g. Schematic representation of co-culture assay performed between isolated neutrophils and Ctl or OS HMEC (ratio 5:1) (left panel). Box plot showing the MFI of degranulation (CD18, CD11b and CD63, n=10) and activation (PD-L1 and ICAM1, n=9) markers in neutrophils after co-culture, assessed by flow cytometry (right panel).

Data information: (**a-b, d-g**) Two-tailed Wilcoxon test. Shown is the median ± SEM. (*p<0.05; **p<0.01; ***p<0.001; ****p<0.0001; ns p≥0.05).

Figure 5: Preneoplastic breast cancer stages involve ER stress and neutrophil recruitment.

a. Anatomopathological characterization of healthy (MMTV-Neu-) and preneoplastic stage (MMTV-Neu+) tissues by Hematoxylin and Eosin staining on Formalin-Fixed Paraffin-Embedded (FFPE) slides.

b., c. Violin plots representing ssGSEA enrichment score of the *Neu*/ERBB2 Signaling Pathway (**b.**) and the UPR (**c.**) signatures in healthy (n=3) and preneoplastic (n=4) epithelial cells in the MMTV-Neu mouse model.

d. Violin plot representing the expression of *cxcl1* in healthy (n=3) and preneoplastic (n=4) epithelial cells in the MMTV-Neu mouse model.

e. Representative Ly6G immunofluorescence staining on FFPE healthy and preneoplastic tissues (left panel). Box plot representing the number of neutrophils per mm^2 in healthy (n=6) and preneoplastic (n=5) tissues (right panel) in the MMTV-Neu mouse model.

f. Principal Component Analysis of luminal epithelial cells from previous wild-type (WT) or pre-cancer stages annotation. WT-like, Stage I and Stage II were manually annotated in BLG-Cre, $BRCA1^{f/f}$, $p53^{+/-}$ mouse model.

g. Dot plot representing ssGSEA enrichment scores of ER stress and UPR response signature in luminal epithelial cells from WT, WT-like, Stage I, and Stage II in the BLG-Cre, $BRCA1^{f/f}$, $p53^{+/-}$ mouse model.

h. Box plot representing the frequency of neutrophil among immune cells in healthy (n=16) and preneoplastic (n=34) tissues in the BLG-Cre, BRCA1f/f, p53+/- mouse model, assessed by flow cytometry.

Data information: (**b-d**) Welch's t test (*p<0.05; **p<0.01). (**e, h**) Two-tailed Wilcoxon test. Shown is the median ± SEM. (**p<0.01).

SUPPLEMENTARY FIGURES

Fig S1: Characteristics of the OS and the OIS stages

a. Images depicting morphological changes in Ctl, OS, Ctl OIS and OIS HMEC (Magnification x20).

b. Quantification of cell size (FSC-A; left panel) and granularity (SSCA-A; right panel) by flow cytometry of dox-treated HMEC-HRas relative to untreated cells at d3 and d5 (n=16).

c. Mean cell number per culture dish of Ctl, OS, Ctl OIS and OIS HMEC (n=36).

d. Representative western blot analysis of proteins involved in the cell cycle using whole cell lysates from a time-course experiment in untreated and dox-treated HMEC-HRas.

e. Senescence-associated beta-galactosidase staining showing by blue coloration (arrow) in Ctl OIS and OIS HMEC.

f. Violin plot representing ssGSEA enrichment score of the Hallmark DNA repair signature in Ctl and OS (n=4) or Ctl OIS and OIS (n=3) HMEC.

g. Violin plots representing the normalized expression of cytokines and chemokines in Ctl and OS (n=4) or Ctl OIS and OIS (n=3) HMEC.

h. Quantification by ELISA of IL8, CXCL1, and GM-CSF production in Ctl OIS and OIS HMEC supernatants. Concentrations were normalized by 10^6 cells (n=6 to 16).

i. Violin plots representing ssGSEA enrichment score of senescent signatures in Ctl OIS and OIS HMEC (n=3).

j. Violin plots representing the normalized expression of NKG2D ligands family genes in Ctl and OS (n=4) or Ctl OIS and OIS (n=3) HMEC.

k. Representative histogram plot of ULBP2-5-6 expression monitored by flow cytometry in Ctl OIS and OIS HMEC (left panel). Box plot illustrating the MFI of the stress ligands expression (right panel) (n=9).

l., m Violin plots representing the normalized expression of CD54/ICAM1 (**l.**) and CD274/PD-L1 (**m.**) genes in Ctl and OS HMEC (n=4).

n. Representative histogram plot of PD-L1 expression monitored by flow cytometry in Ctl OIS and OIS HMEC (left panel). Box plot illustrating the MFI of PD-L1 expression (right panel) (n=9).

Data information: (**b, h, k, n**) Two-tailed Wilcoxon test. Shown is the median ± SEM (*p<0.05; **p<0.01; ***p<0.001; ****p<0.0001). (**c**) Two-Way ANOVA test (**p<0.01). (**f, g, j**) One-Way ANOVA test (*p<0.05; **p<0.01; ***p<0.001; ****p<0.0001; ns p≥0.05). (**i, l-m**) Mann-Whitney test (*p<0.05; **p<0.01; ***p<0.001).

Fig S2: UPR pathways are specifically activated by the OS

a. Scheme of the Unfolded Protein Response (UPR) pathways

b., c. Violin plots representing ssGSEA enrichment score of the ER stress Response (**b.**) or the IRE1 (left panel), PERK (central panel) and ATF6 (right panel) pathways (**c.**) signatures in Ctl OIS and OIS HMEC (n=3)

d. Box plots representing IRE1 target gene (*dnajb9*) and PERK target genes (*chop* and *ppp1r15a*) expression measured by RT-qPCR and normalized on Ctl OIS HMEC.

e., f. HMEC-GFP model was developed as a control for HRas overexpression. Box plot showing the MFI of the GFP expression in untreated (-Dox) or dox-treated (+Dox) HMEC-GFP at d3, assessed by

flow cytometry (**e.**). Box plots representing IRE1 target genes (*dnajb9* and *xbp1s*) and PERK target genes (*chop* and *ppp1r15a*) expression measured by RT-qPCR and normalized on untreated HMEC-GFP at d3 (**f.**).

g. Scheme representing the protocol performed to investigate whether physiological activation of the Ras signaling pathway could elicit the same intrinsic response. HMEC-HRas cultures were supplemented with EGF at different concentrations (5, 20, and 100 ng/mL) and analyzed over time (0.5, 6, 12, 24, and 72h). For the 72-hour time point, the medium was refreshed every 24 hours with EGF at the respective concentrations.

h. Representative western blot analysis of Ras and its downstream factor ERK using whole cell lysates from a time-course experiment in untreated, dox-treated and EGF-treated HMEC-HRas at d3.

i. Box plots representing IRE1 target genes (*dnajb9*) and PERK target genes (*chop* and *ppp1r15a*) expression measured by RT-qPCR and normalized on Ctl HMEC.

j. Scheme representing the protocol performed, given that glucose deprivation is another factor capable of activating the UPR pathways. HMEC-HRas cultures were supplemented with exogenous glucose (20 mM) on d2.

k. Bar plot representing the quantification of the glucose concentration in Ctl and OS HMEC supernatants (n=2). The dashed line represents 5mM of glucose, representing a critical concentration that can induce ER stress.

l. Box plots representing IRE1 target genes (*dnajb9* and *xbp1s*) and PERK target genes (*chop* and *ppp1r15a*) expression measured by RT-qPCR and normalized on Ctl HMEC in presence or not of glucose, respectively.

Data information: (**b-c**) Mann-Whitney test (*p<0.05; **p<0.01; ***p<0.001; ns p≥0.05). (**d-f**) Two-tailed Wilcoxon test. Shown is the median ± SEM (*p<0.05; ns p≥0.05). (**l**) Friedman test (*p<0.05; ns p≥0.05).

Fig S3: Validation of the pharmacological inhibition of PERK and IRE1 pathways

a. Scheme representing the pharmacological inhibition of PERK (GSK-2606414) and IRE1 (4µ8c) pathways.

b. Box plots representing IRE1 target genes (*dnajb9*) and PERK target genes (*chop* and *ppp1r15a*) expression measured by RT-qPCR and normalized on Ctl HMEC in presence or not of pharmacological inhibitors (GSK-2606414 and 4µ8c), respectively.

Data information: (**b**) Kruskall-Wallis test. Shown is the median ± SEM. (**p<0.01; ***p<0.001 ; ****p<0.0001; ns p≥0.05).

Fig S4: Immune cell recruitment by OS cells *in vitro* and in *in vivo* matrigrel

a. Schematic representation of transwell assays performed with using peripheral blood mononuclear cells (PBMCs) (left panel). Box plot showing the recruitment of PBMCs populations by Ctl or OS HMEC normalized supernatants monitored by flow cytometry (right panel) (n=14).

b. Scheme of the matrigel assay *in vitro*: HMEC were embedded in matrigel without or with dox in the culture medium and then cultured *in vitro*. Upon $HRas^{G12V}$ induction, the OS (d3) and the OIS (d5) stages are determined.

c. Representative western blot analysis of Ras and its downstream factor ERK using whole cell lysates from a time-course experiment in untreated and treated matrigel at d3 and d5.

d. Bar plot representing the cell number per matrigel containing Ctl, OS, Ctl OIS and OIS HMEC (n=1).

e. Bar plot representing the quantification by ELISA of IL-8 and GM-CSF production in matrigel containing Ctl, OS, Ctl OIS and OIS HMEC. Concentrations were normalized for 10^6 cells (n=1).

f. Box plots representing the frequency (left panel) or the number (right panel) of immune cells among viable cells in matrigel containing Ctl or OS HMEC, assessed by flow cytometry (n=7).

Data information: (**a, f**) Two-tailed Wilcoxon test. Shown is the median ± SEM. (ns $p \geq 0.05$).

Fig S5: ERBB2 expression and immune cell recruitment at preneoplastic stage

a. Violin plot representing the expression of *neu/erbb2/her2* in healthy (n=3) and preneoplastic (n=4) epithelial cells in the MMTV-Neu mouse model.

b. Box plot representing the frequency of immune cells among viable cells in healthy (n=16) and preneoplastic stage (n=34) tissues in BLG-Cre, $BRCA1^{f/f}$, $p53^{+/-}$ mouse model assessed by flow cytometry.

Data information: (**a**) Welch's t test (****$p<0.0001$) (**b**) Two-tailed Wilcoxon test. Shown is the median ± SEM. (**$p<0.01$).

SUPPLEMENTARY TABLES

Table S1: Differential Expressed Genes between OS vs Ctl HMEC with subcellular localization of the corresponding proteins (see supplementary excel files : loc_deg_os)

Table S2: Panels of antibodies for cytometry assays

a. Antibodies for Flow cytometry BRCA1 model	Manufacturer	Reference	Clone	Dilution
BV711 anti-mouse CD8a	Biolegend	100747	53-6.7	1:200
BV650 anti-mouse CD3	BD	564378	145-2C11	1:50
Zombie Aqua	Biolegend	423102		1:400
V450 anti-mouse CD19	BD	560376	1D3	1:50
FITC anti-mouse Ly6G	BD	551460	1A8	1:100
PE anti-mouse Siglec F	BD	552126	E50-2440	1:100
PE-Cy7 anti-mouse FoxP3	eBioscience	25-5773-82	FJK-16s	1:100
PE-Cy5 anti-mouse CD4	BD	553654	H129.19	1:200
PE-Dazzle 594 anti-mouse CD64	Biolegend	139319	X54-5/7.1	1:200
APC anti-mouse CD49b	BD	560628	DX5	1:50
Alexa Fluor 700 anti-mouse CD45	Biolegend	103128	30-F11	1:400

b. Antibodies for Cell sorting MMTV-Neu model	Manufacturer	Reference	Clone	Dilution
Purified anti-mouse CD16/32	Biolegend	101302	93	1:50
FITC anti-mouse Ly6G	BD	551460	1A8	1:400
PE anti-mouse Siglec F	BD	552126	E50-2440	1:100
PE-Cy7 anti-mouse CD326	Biolegend	118216	G8.8	1:200
APC anti-mouse CD3	Biolegend	100236	17A2	1:100
APC anti-mouse CD4	Biolegend	100412	GK1.5	1:400
APC anti-mouse CD8a	Biolegend	100712	53-6-7	1:200
APC anti-mouse CD11c	BD	550261	HL3	1:100
APC anti-mouse CD19	Biolegend	115512	6D5	1:200
APC anti-mouse CD335	Biolegend	137608	29A1.4	1:100
APC anti-mouse TER-119	Biolegend	116212	TER-119	1:200
Alexa Fluor 700 anti-mouse CD45.2	Biolegend	109822	104	1:400
APC-Cy7 anti-mouse Ly6C	BD	560596	AI-21	1:200

c. Antibodies for Transwell Migration Assay (Isolated Neutrophils)	Manufacturer	Reference	Clone	Dilution
BV421 anti-human CD66b	BD	562940	G10F5	1:30
PE-CF594 anti-human CD15	BD	562485	MC480	1:50
Alexa Fluor 700 anti-human CD45	BD	560566	HI30	1:25
Zombie NIR	Biolegend	423106		1:800

d. Antibodies for Transwell Migration Assay (Total immune cells and PBMCs)	Manufacturer	Reference	Clone	Dilution
BUV395 anti-human CD45	BD	563792	HI30	1:50
Live/Dead Blue	Thermofisher	L34962		1:500
BUV737 anti-human CD89	BD	749244	A59	1:20
BUV805 anti-human CD15	BD	742057	W6D3	1:20
BV421 anti-human CD3	Biolegend	300434	UCHT1	1:50
BV711 anti-human CD4	BD	563028	SK3	1:50
BV750 anti-human CD56	Biolegend	362556	5.1H11	1:20
BB515 anti-human CD20	BD	564568	2H7	1:100
PerCP-Cy5.5 anti-human CD11c	Biolegend	337210	Bu15	1:50
PE anti-human CD66b	Miltenyi	130-104-396	REA 306	1:100
PE-Dazzle 594 anti-human CD123	Biolegend	306034	6H6	1:40
PE-Cy7 anti-human CD19	BD	557835	SJ25C1	1:50
APC anti-human CD14	BD	555399	M5E2	1:25
Alexa Fluor 700 anti-human CD8	BD	557945	RPA-T8	1:25
APC-H7 anti-human HLA-DR	BD	561358	G46-6	1:50

e. Antibodies for p-STAT5 Activation	Manufacturer	Reference	Clone	Dilution
BV421 anti-human CD66b	BD	562940	G10F5	1:30
V500 anti-human CD15	BD	561585	HI98	1:50
BV711 anti-human CD14	Biolegend	301838	M5E2	1:25
PE-CF594 anti-human p-STAT5	BD	562501	47	1:100
APC anti-human Siglec8	Miltenyi	130-117-975	REA1045	1:50
Alexa Fluor 700 anti-human CD45	BD	560566	HI30	1:25
Zombie NIR	Biolegend	423106		1:800

f. Antibodies for ROS Production	Manufacturer	Reference	Clone	Dilution
BV421 anti-human CD66b	BD	562940	G10F5	1:30
PE-CF594 anti-human CD15	BD	562485	MC480	1:50
Alexa Fluor 700 anti-human CD45	BD	560566	HI30	1:25
Zombie NIR	Biolegend	423106		1:800

g. Antibodies for Co-culture Assay	Manufacturer	Reference	Clone	Dilution
BV421 anti-human CD18	BD	743370	6.7	1:20
BV711 anti-human CD11b	BD	740771	ICRF4	1:20
FITC anti-human CD66b	BD	555724	G10F5	1:40
PE anti-human ULBP2-5-6	R&D	FAB1298P	165903	1:2,5
PE-CF594 anti-human CD63	BD	565403	H5C6	1:50
PE-Cy7 anti-human PD-L1	Biolegend	329718	29E2A3	1:50
APC anti-human ICAM1	Miltenyi	130-121-342	REA266	1:11
Alexa Fluor 700 anti-human CD45	BD	560566	HI30	1:25
Zombie NIR	Biolegend	423106		1:800

h. Antibodies for *In Vivo* Matrigel Plug Assay	Manufacturer	Reference	Clone	Dilution
BUV395 anti-mouse CD11b	BD	563553	M1/70	1:100
BV421 anti-mouse PD-L1	Biolegend	124315	10F.9G2	1:100
BV605 anti-mouse CD54	BD	740343	3E2	1:200
BV786 anti-mouse CD62L	BD	564109	MEL-14	1:400
Vio B515 anti-mouse CD107a	Miltenyi	130-111-320	REA777	1:100
PerCP vio 770 anti-mouse Ly6G	Miltenyi	130-117-500	REA526	1:50
PE anti-mouse SiglecF	BD	552126	E50-2440	1:100
PE-Dazzle 594 anti-mouse CD3	Biolegend	100348	145-2C11	1:25
PE-Dazzle 594 anti-mouse CD19	Biolegend	115554	6D5	1:10
PE-Dazzle 594 anti-mouse CD64	Biolegend	139319	X54-5/7.1	1:100
PE-Vio 770 anti-mouse CD69	Miltenyi	130-115-577	REA937	1:100
APC anti-mouse NK1.1	Biolegend	108710	PK136	1:100
Alexa Fluor 700 anti-mouse CD45	Biolegend	103128	30-F11	1:200
ViaKrome 808	Beckman	C36628		1:40

i. Antibodies for HMEC membrane ligands	Manufacturer	Reference	Clone	Dilution
PE anti-human ULBP2-5-6	R&D	FAB1298P	165903	1:2,5
PE-Cy7 anti-human PD-L1	Biolegend	329718	29E2A3	1:50
APC anti-human ICAM1	Miltenyi	130-121-342	REA266	1:11
Zombie NIR	Biolegend	423106		1:800

Table S3: Gene sets (MSigDB)

a. ssGSEA analysis Geneset (Mouse models)	Species	Collection
HALLMARK_UNFOLDED_PROTEIN_RESPONSE	Mouse	MH
REACTOME_UNFOLDED_PROTEIN_RESPONSE_UPR	Mouse	M2
GOBP_ENDOPLASMIC_RETICULUM_UNFOLDED_PROTEIN_RESPONSE	Mouse	M5
GOBP_ERBB2_SIGNALING_PATHWAY	Mouse	M5
GOBP_RESPONSE_TO_ENDOPLASMIC_RETICULUM_STRESS	Mouse	M5

b. ssGSEA analysis (HMEC model)	Species	Collection
HALLMARK_DNA_REPAIR	Human	H
BILD_HRAS_ONCOGENIC_SIGNATURE	Human	C2-CPG
FRIDMAN_SENESCENCE_UP	Human	C2-CPG
SAUL_SEN_MAYO	Human	C2-CPG
GOBP_ATF6_MEDIATED_UNFOLDED_PROTEIN_RESPONSE	Human	C5
GOBP_IRE1_MEDIATED_UNFOLDED_PROTEIN_RESPONSE	Human	C5
GOBP_PERK_MEDIATED_UNFOLDED_PROTEIN_RESPONSE	Human	C5
GOBP_REGULATION_OF_RESPONSE_TO_STRESS	Human	C5
GOBP_RESPONSE_TO_ENDOPLASMIC_RETICULUM_STRESS	Human	C5
GOBP_RESPONSE_TO_TYPE_I_INTERFERON	Human	C5

Table S4: Panel of antibodies for Multiplex Immunofluorescence

Antibodies for mIF	Manufacturer	Reference	Clone	Dilution
Anti-mouse CD45	Cell Signaling	70257	D3F8Q	1:300
Anti-mouse CD326	Abcam	ab71916	Polyconal	1:500
anti-mouse Ly6G	Cell Signaling	87048S	E6Z1T	1:300

Table S5: Antibodies for western blotting

Antibodies for Western Blot	Manufacturer	Reference	Host	Clone	Dilution
Ras	Santa-Cruz	sc-520	Rabbit	C-20	1:1000
ERK	Cell signaling	9102	Rabbit	Polyclonal	1:1000
p-ERK	Cell signaling	9101	Rabbit	Polyclonal	1:1000
KAP1	Bethyl	A300-275A	Rabbit	Polyclonal	1:1000
p-KAP1	Bethyl	A300-767A-M	Rabbit	Polyclonal	1:5000
CHK1	Cell signaling	2360	Mouse	2G1D5	1:1000
p-CHK1	Cell signaling	2348	Rabbit	133D3	1:1000
CHK2	Cell signaling	3440	Mouse	1C12	1:1000
p-CHK2	Cell signaling	2661	Rabbit	Polyclonal	1:1000
H2A.X	Millipore	07-627	Rabbit	Polyclonal	1:1000
p-H2A.X	Millipore	05-636	Mouse	JBW301	1:1000
PERK	Cell signaling	3192S	Rabbit	C33E10	1:1000
p-eif2α	Cell signaling	9722S	Rabbit	Polyclonal	1:1000
IRE1α	Cell signaling	3294P	Rabbit	14C10	1:1000
ATF6	Abcam	ab122897	Mouse	1-7	1:1000
Cyclin A	Santa-Cruz	sc-751	Mouse	H-432	1:5000
Cycline B1	Santa-Cruz	sc-245	Mouse	GNS1	1:1000
Cyclin D1	Santa-Cruz	sc-246	Mouse	HD11	1:1000
Cyclin D3	Santa-Cruz	sc-182	Rabbit	C-16	1:250
Cyclin E	Santa-Cruz	sc-247	Mouse	HE12	1:500
Cdk1	Santa-Cruz	sc-54	Mouse	17	1:500
Cdk2	Santa-Cruz	sc-163	Rabbit	M2	1:1000
Cdk4	Santa-Cruz	sc-260	Rabbit	C-22	1:2000
Cdk6	Santa-Cruz	sc-177	Rabbit	C-21	1:2000
β-actin	MP Biomedicals	69100	Mouse	C4	1:50000
αTubulin	Sigma-Aldrich	T5168	Mouse	B-5-1-2	1:2500

Table S6: Primers for RT-qPCR

Primers for RT-qPCR	Manufacturer	Forward primer	Reverse Primer
GUS primers	Eurogentech	5' CGTGGTTGGAGAGCTCATTTGGAA 3'	5' ATTCCCCAGCACTCTCGTCGGT 3'
DNAJB9 primers	Eurogentech	5' TCTTAGGTGTGCCAAAATCGG 3'	5' TGTCAGGGTGGTACTTCATGG 3'
HERPUD primers	Eurogentech	5' CAAAAATGCCAGAAATCAACG 3'	5' CTGTCCCCGATTAGAACCAG 3'
HRD1 primers	Eurogentech	5' CCAGTACCTCACCGTGCTG 3'	5' GCCTCTGAGCTAGGGATGC 3'
XBP1s primers	Eurogentech	5' CTGAGTCCGAATCAGGTGCAG 3'	5' ATCCATGGGGAGATGTTCTGG 3'

PPP15R1A primers	Eurogentech	5’ GCTTCTGGCAGACCGAAC 3’	5’ GTAGCCTGATGGGGTGCTT 3’
CHOP primers	Eurogentech	5’ CAGAGCTGGAACCTGAGGAG 3’	5’ TGGATCAGTCTGGAAAAGCA 3’
RIG-I primers	Eurogentech	5’ AGCTCAGCTTGATGAGGGACA 3’	5’ GTCTGGCATCTGGAACACCA 3’
ISG20 primers	Eurogentech	5’ CACCCCTCAGCACATGGT 3’	5’ TGGAAGTCGTGCTTCAGGT 3’
IRF7 primers	Eurogentech	5’ CAAGTGCAAGGTGTACTGG 3’	5’ CAGGTAGATGGTATAGCGTGG 3’
IRF9 primers	Eurogentech	5’ CATGCAGAACTGCACACTCA 3’	5’ CCAATGTCTGAATGGACTGC 3’
SOCS1 primers	Eurogentech	5’ TTTTCGCCCTTAGCGTGAAGA 3’	5' GAGGCAGTCGAAGCTCTCG 3'

Table S7: Kits ELISA

Kits ELISA	Manufacturer	Reference
Human GM-CSF DuoSet ELISA	R&D Systems™ - Bio-Techne	DY215
Human CXCL1/GRO alpha DuoSet ELISA	R&D Systems™ - Bio-Techne	DY275
Human G-CSF DuoSet ELISA	R&D Systems™ - Bio-Techne	DY214
Human CXCL2/GRO beta DuoSet ELISA	R&D Systems™ - Bio-Techne	DY276
Human GROγ/CXCL3 ELISA Kit (home-made kit) Recombinant human GROγ Cat300-40 Biotinylated rabbit anti-human GROγ Cat500-P105Bt	Peprotech	
Human IL-8 (CXCL8) Standard ABTS ELISA Development Kit	Peprotech	900-K18

Figure 1

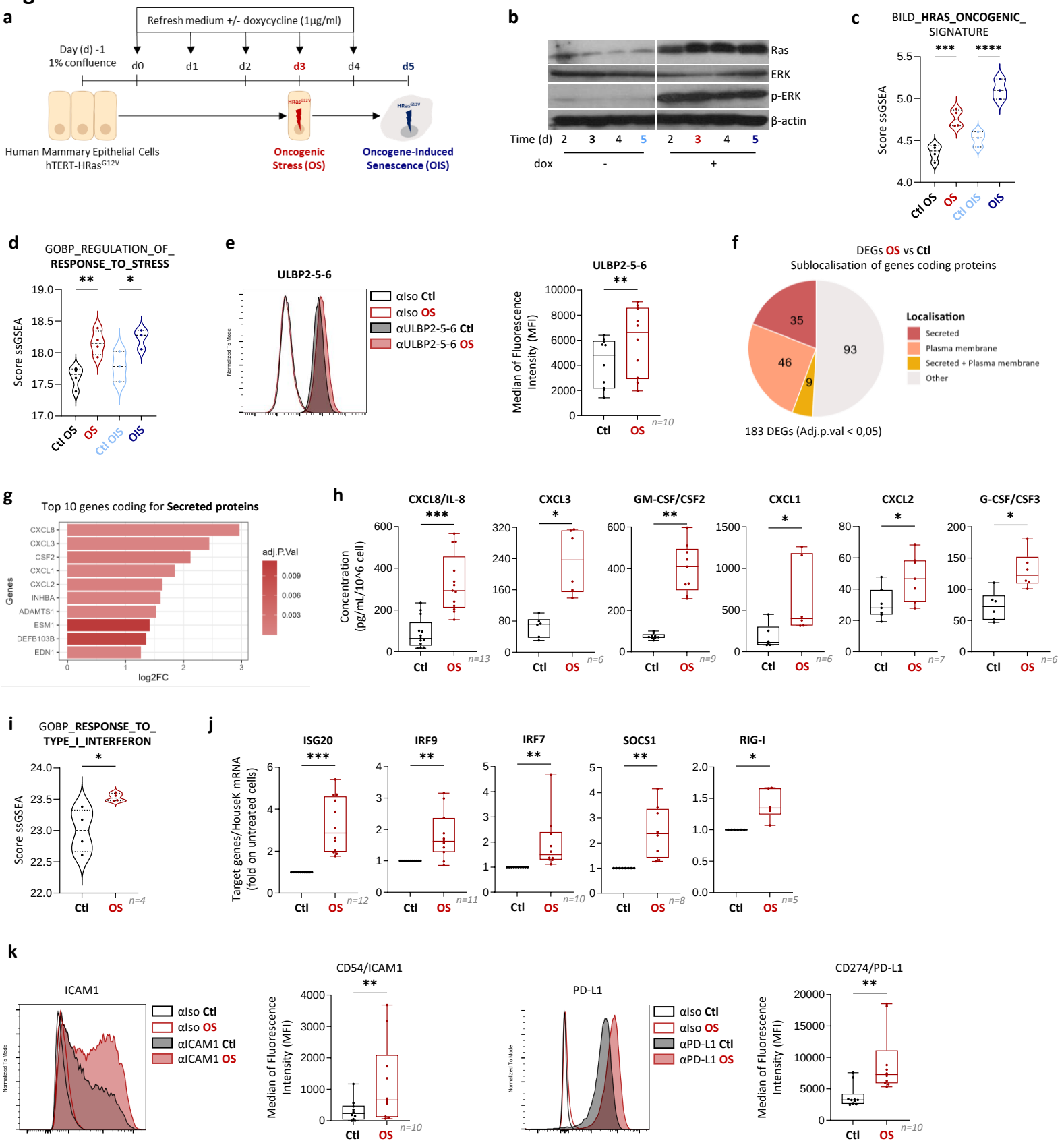
a
Refresh medium +/- doxycycline (1µg/ml)
Day (d) -1
1% confluence
d0
d1
d2
d3
d4
d5
Human Mammary Epithelial Cells
hTERT-HRas^{G12V}
Oncogenic
Stress (OS)
Oncogene-Induced
Senescence (OIS)
b
Ras
ERK
p-ERK
β-actin
Time (d) 2 3 4 5 2 3 4 5
dox - +
c
BILD_HRAS_ONCOGENIC_
SIGNATURE
Score ssGSEA
Ctl OS
OS
Ctl OIS
OIS
d
GOBP_REGULATION_OF_
RESPONSE_TO_STRESS
Score ssGSEA
e
ULBP2-5-6
αIso Ctl
αIso OS
αULBP2-5-6 Ctl
αULBP2-5-6 OS
Median of Fluorescence
Intensity (MFI)
n=10
f
DEGs OS vs Ctl
Sublocalisation of genes coding proteins
Localisation
Secreted
Plasma membrane
Secreted + Plasma membrane
Other
183 DEGs (Adj.p.val < 0,05)
g
Top 10 genes coding for Secreted proteins
Genes
CXCL8
CXCL3
CSF2
CXCL1
CXCL2
INHBA
ADAMTS1
ESM1
DEFB103B
EDN1
adj.P.Val
log2FC
h
CXCL8/IL-8
CXCL3
GM-CSF/CSF2
CXCL1
CXCL2
G-CSF/CSF3
Concentration
(pg/mL/10^6 cell)
i
GOBP_RESPONSE_TO_
TYPE_I_INTERFERON
Score ssGSEA
j
ISG20
IRF9
IRF7
SOCS1
RIG-I
Target genes/HouseK mRNA
(fold on untreated cells)
k
ICAM1
αIso Ctl
αIso OS
αICAM1 Ctl
αICAM1 OS
CD54/ICAM1
Median of Fluorescence
Intensity (MFI)
PD-L1
αIso Ctl
αIso OS
αPD-L1 Ctl
αPD-L1 OS
CD274/PD-L1

Figure S1

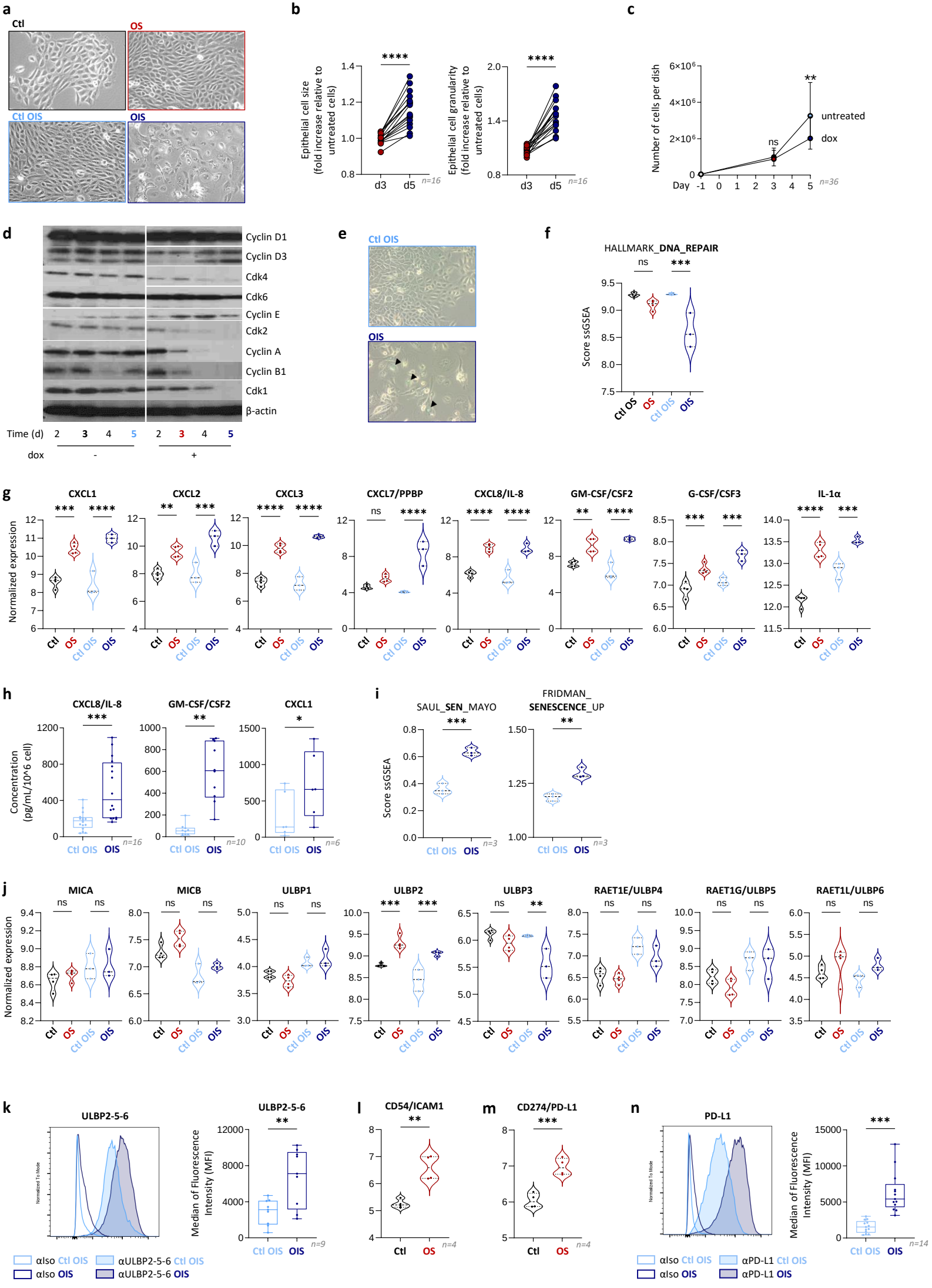
a
Ctl
OS
Ctl OIS
OIS
b
Epithelial cell size (fold increase relative to untreated cells)
Epithelial cell granularity (fold increase relative to untreated cells)
****
d3
d5
n=16
c
Number of cells per dish
untreated
dox
ns
**
Day
n=36
d
Cyclin D1
Cyclin D3
Cdk4
Cdk6
Cyclin E
Cdk2
Cyclin A
Cyclin B1
Cdk1
β-actin
Time (d)
dox
e
Ctl OIS
OIS
f
HALLMARK_DNA_REPAIR
Score ssGSEA
g
CXCL1
CXCL2
CXCL3
CXCL7/PPBP
CXCL8/IL-8
GM-CSF/CSF2
G-CSF/CSF3
IL-1α
Normalized expression
h
CXCL8/IL-8
GM-CSF/CSF2
CXCL1
Concentration (pg/mL/10^6 cell)
n=16
n=10
n=6
i
SAUL_SEN_MAYO
FRIDMAN_SENESCENCE_UP
Score ssGSEA
n=3
j
MICA
MICB
ULBP1
ULBP2
ULBP3
RAET1E/ULBP4
RAET1G/ULBP5
RAET1L/ULBP6
Normalized expression
k
ULBP2-5-6
Median of Fluorescence Intensity (MFI)
αIso Ctl OIS
αIso OIS
αULBP2-5-6 Ctl OIS
αULBP2-5-6 OIS
n=9
l
CD54/ICAM1
n=4
m
CD274/PD-L1
n=4
n
PD-L1
αIso Ctl OIS
αIso OIS
αPD-L1 Ctl OIS
αPD-L1 OIS
n=14

Figure 2

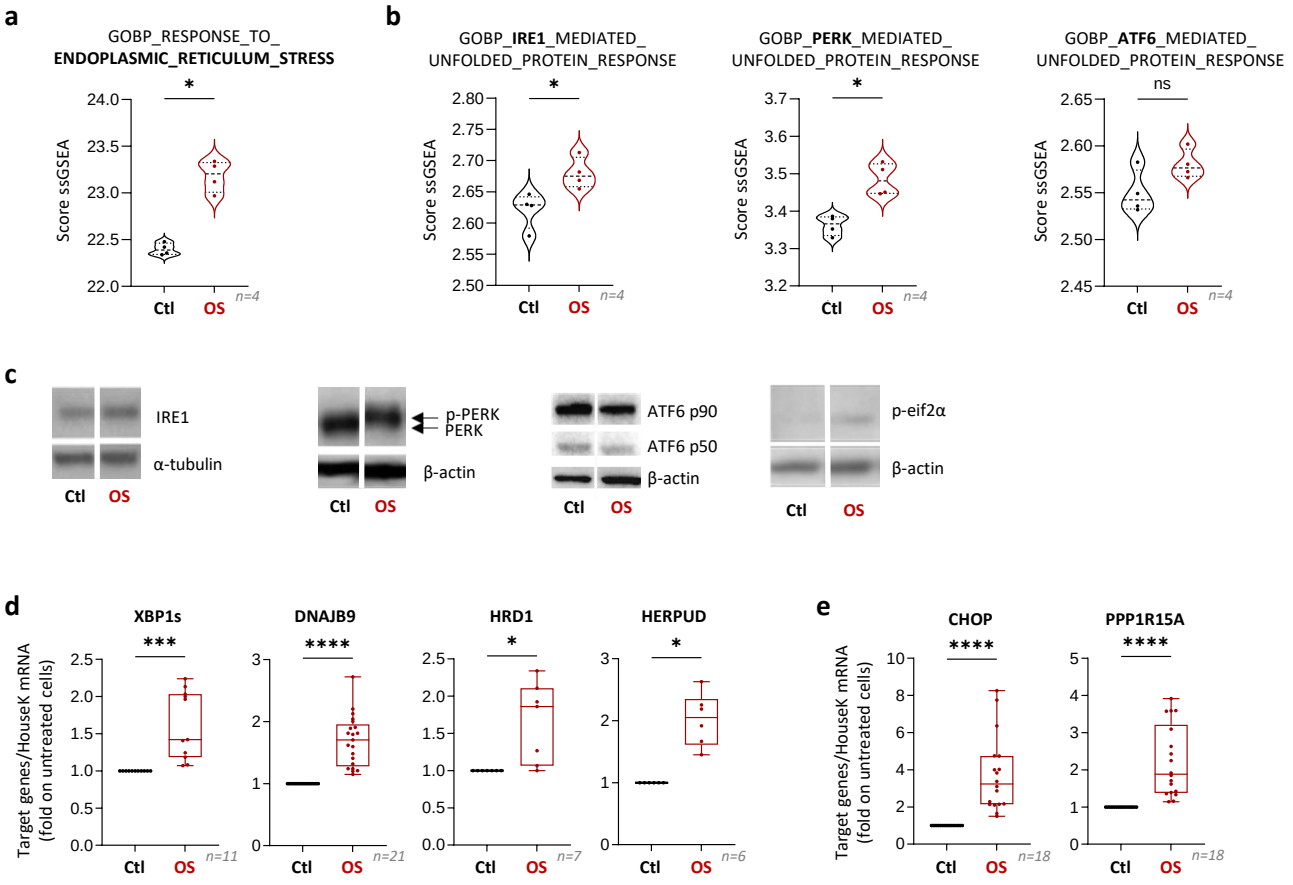
a
GOBP_RESPONSE_TO_
ENDOPLASMIC_RETICULUM_STRESS
Score ssGSEA
Ctl
OS
n=4
b
GOBP_IRE1_MEDIATED_
UNFOLDED_PROTEIN_RESPONSE
GOBP_PERK_MEDIATED_
UNFOLDED_PROTEIN_RESPONSE
GOBP_ATF6_MEDIATED_
UNFOLDED_PROTEIN_RESPONSE
ns
c
IRE1
α-tubulin
p-PERK
PERK
β-actin
ATF6 p90
ATF6 p50
p-eif2α
d
XBP1s
DNAJB9
HRD1
HERPUD
Target genes/HouseK mRNA
(fold on untreated cells)
n=11
n=21
n=7
n=6
e
CHOP
PPP1R15A
n=18

Figure S2

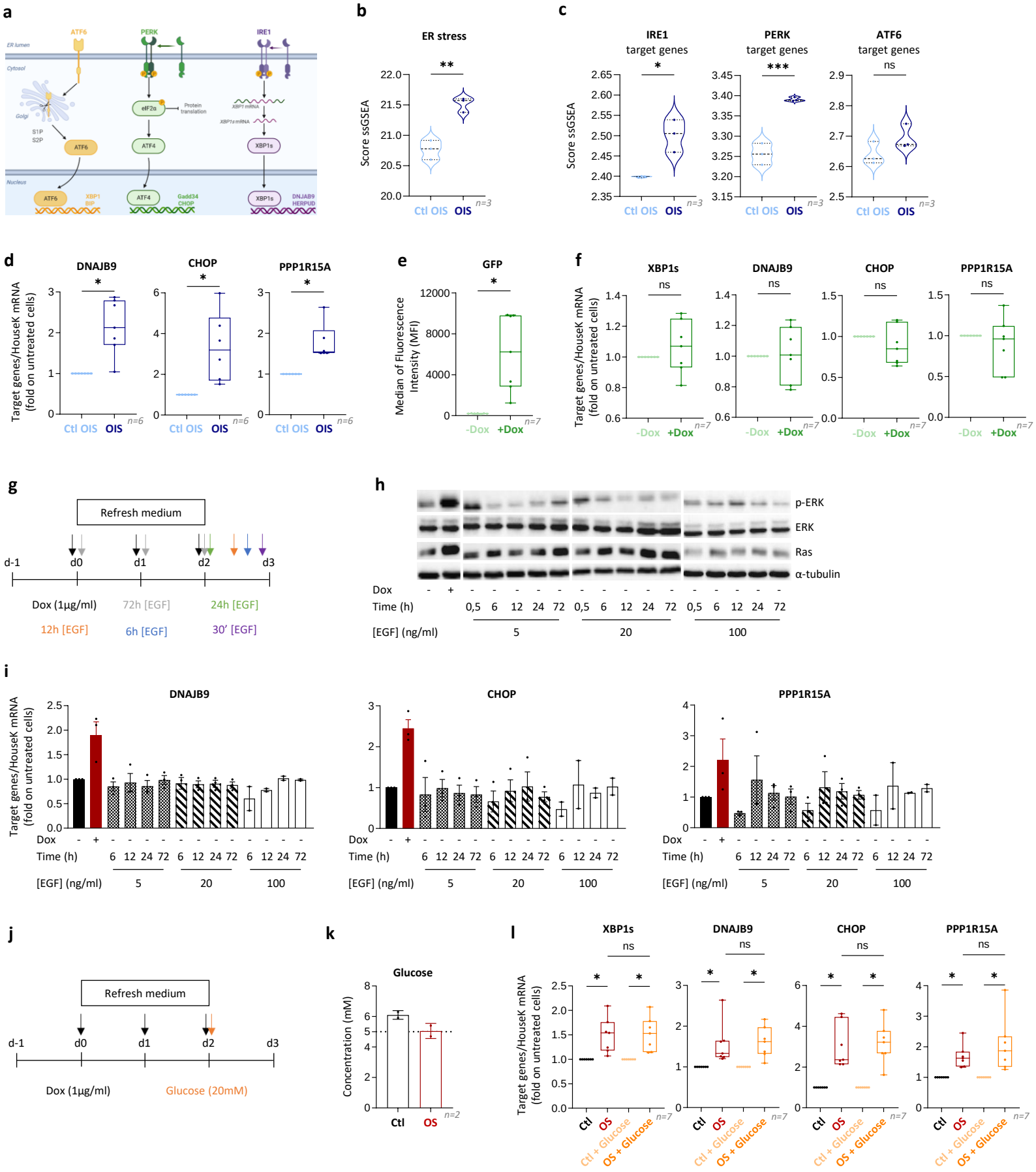
a
ATF6
PERK
IRE1
ER lumen
Cytosol
Golgi
S1P
S2P
eIF2α
Protein translation
XBP1 mRNA
XBP1s mRNA
ATF6
ATF4
XBP1s
Nucleus
ATF6
XBP1
BIP
ATF4
Gadd34
CHOP
XBP1s
DNJAB9
HERPUD
b
ER stress
Score ssGSEA
Ctl OIS
OIS
n=3
c
IRE1 target genes
PERK target genes
ATF6 target genes
Score ssGSEA
Ctl OIS
OIS
n=3
d
DNAJB9
CHOP
PPP1R15A
Target genes/HouseK mRNA (fold on untreated cells)
Ctl OIS
OIS
n=6
e
GFP
Median of Fluorescence Intensity (MFI)
-Dox
+Dox
n=7
f
XBP1s
DNAJB9
CHOP
PPP1R15A
Target genes/HouseK mRNA (fold on untreated cells)
-Dox
+Dox
n=7
g
Refresh medium
d-1
d0
d1
d2
d3
Dox (1µg/ml)
72h [EGF]
24h [EGF]
12h [EGF]
6h [EGF]
30' [EGF]
h
p-ERK
ERK
Ras
α-tubulin
Dox
Time (h)
0,5 6 12 24 72 0,5 6 12 24 72 0,5 6 12 24 72
[EGF] (ng/ml)
5
20
100
i
DNAJB9
CHOP
PPP1R15A
Target genes/HouseK mRNA (fold on untreated cells)
Dox
Time (h)
6 12 24 72 6 12 24 72 6 12 24 72
[EGF] (ng/ml)
5
20
100
j
Refresh medium
d-1
d0
d1
d2
d3
Dox (1µg/ml)
Glucose (20mM)
k
Glucose
Concentration (mM)
Ctl
OS
n=2
l
XBP1s
DNAJB9
CHOP
PPP1R15A
ns
Target genes/HouseK mRNA (fold on untreated cells)
Ctl
OS
Ctl + Glucose
OS + Glucose
n=7

Figure 3

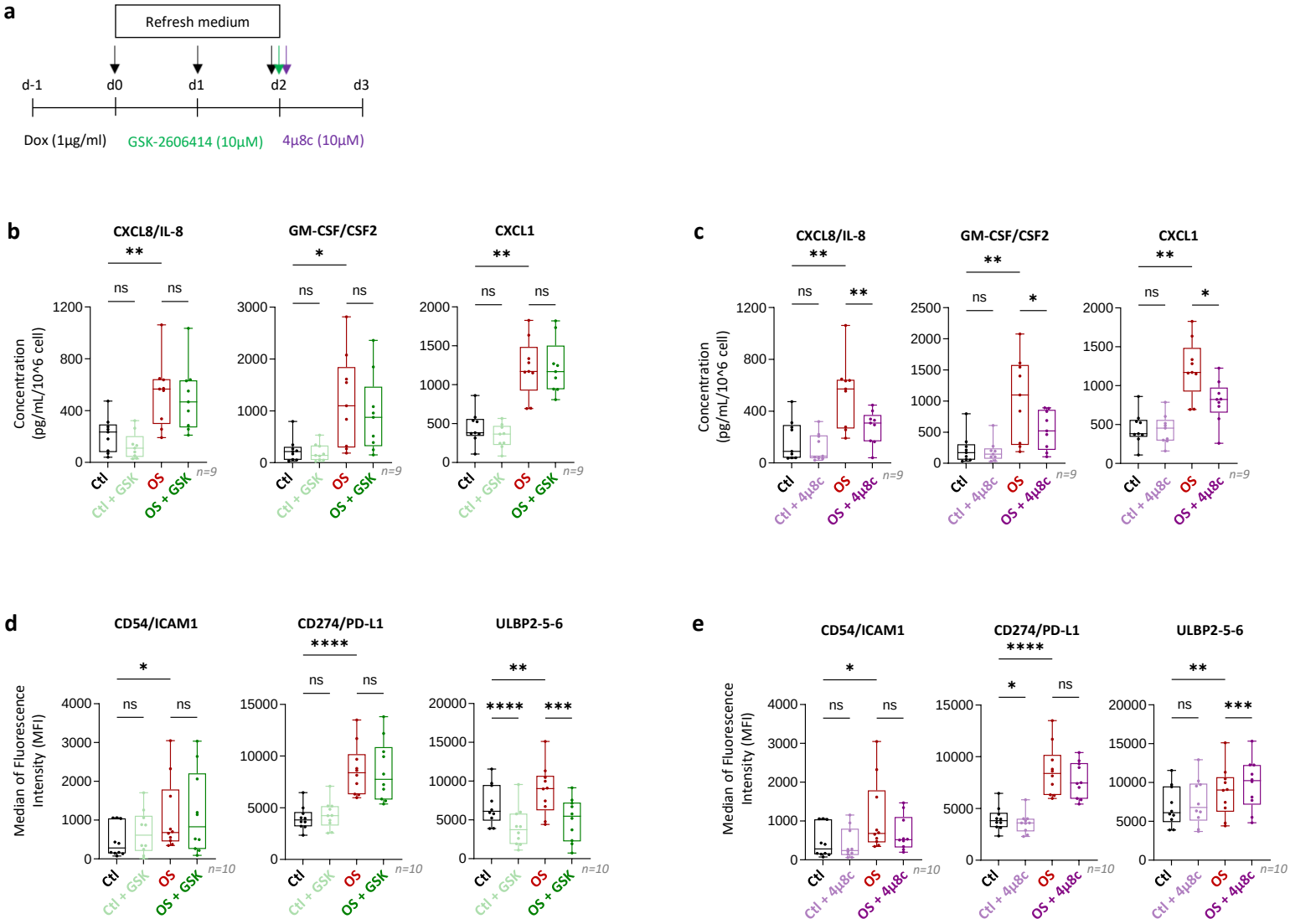
a
Refresh medium
d-1
d0
d1
d2
d3
Dox (1µg/ml)
GSK-2606414 (10µM)
4µ8c (10µM)
b
CXCL8/IL-8
GM-CSF/CSF2
CXCL1
Concentration (pg/mL/10^6 cell)
Ctl
Ctl + GSK
OS
OS + GSK
n=9
c
CXCL8/IL-8
GM-CSF/CSF2
CXCL1
Concentration (pg/mL/10^6 cell)
Ctl
Ctl + 4µ8c
OS
OS + 4µ8c
n=9
d
CD54/ICAM1
CD274/PD-L1
ULBP2-5-6
Median of Fluorescence Intensity (MFI)
Ctl
Ctl + GSK
OS
OS + GSK
n=10
e
CD54/ICAM1
CD274/PD-L1
ULBP2-5-6
Median of Fluorescence Intensity (MFI)
Ctl
Ctl + 4µ8c
OS
OS + 4µ8c
n=10

Figure S3

a

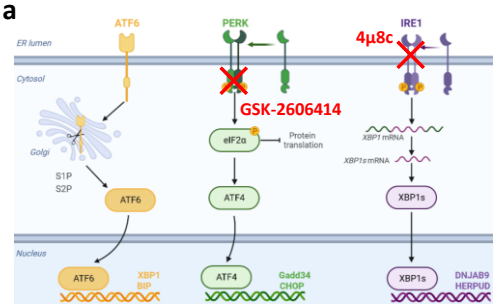
ATF6
PERK
IRE1
4µ8c
ER lumen
Cytosol
GSK-2606414
eIF2α
Protein translation
XBP1 mRNA
XBP1s mRNA
Golgi
S1P
S2P
ATF6
ATF4
XBP1s
Nucleus
ATF6
XBP1
BIP
ATF4
Gadd34
CHOP
XBP1s
DNJAB9
HERPUD

b

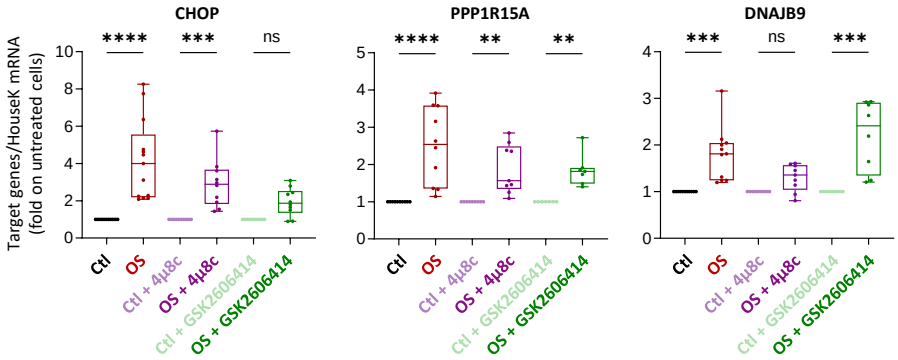
CHOP
PPP1R15A
DNAJB9
Target genes/HouseK mRNA
(fold on untreated cells)
****
***
ns
****
**
**
***
ns
***
Ctl
OS
Ctl + 4µ8c
OS + 4µ8c
Ctl + GSK2606414
OS + GSK2606414

Figure 4

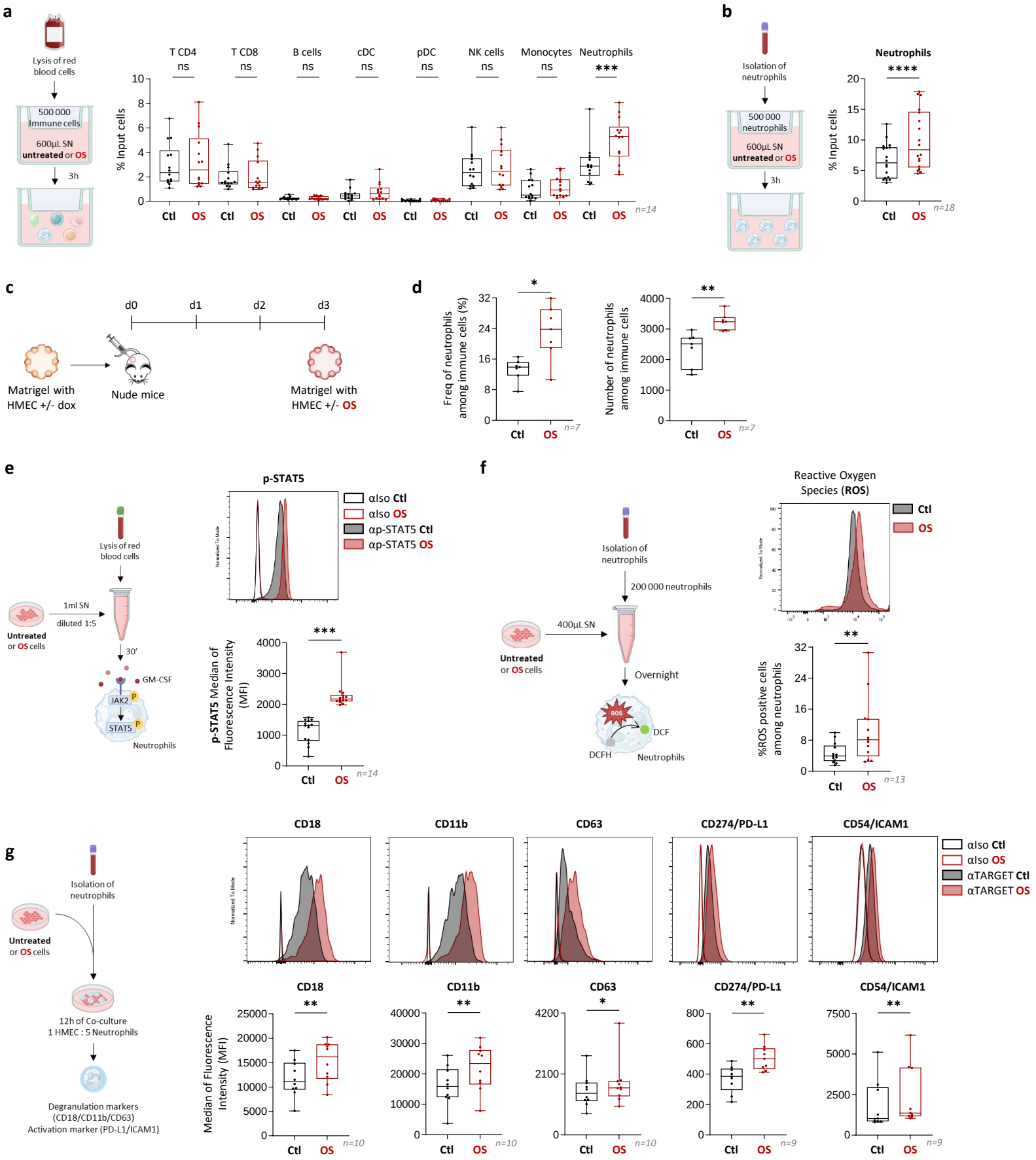
a
Lysis of red blood cells
500 000 Immune cells
600µL SN untreated or OS
3h
T CD4 ns
T CD8 ns
B cells ns
cDC ns
pDC ns
NK cells ns
Monocytes ns
Neutrophils ***
% Input cells
Ctl OS Ctl OS Ctl OS Ctl OS Ctl OS Ctl OS Ctl OS Ctl OS
n=14
b
Isolation of neutrophils
500 000 neutrophils
600µL SN untreated or OS
3h
Neutrophils ****
% Input cells
Ctl OS
n=18
c
d0 d1 d2 d3
Matrigel with HMEC +/- dox
Nude mice
Matrigel with HMEC +/- OS
d
Freq of neutrophils among immune cells (%)
*
Ctl OS
n=7
Number of neutrophils among immune cells
**
Ctl OS
n=7
e
Lysis of red blood cells
1ml SN diluted 1:5
Untreated or OS cells
30'
GM-CSF
JAK2
STAT5
Neutrophils
p-STAT5
αIso Ctl
αIso OS
αp-STAT5 Ctl
αp-STAT5 OS
p-STAT5 Median of Fluorescence Intensity (MFI)
***
Ctl OS
n=14
f
Isolation of neutrophils
200 000 neutrophils
400µL SN
Untreated or OS cells
Overnight
ROS
DCF
DCFH
Neutrophils
Reactive Oxygen Species (ROS)
Ctl
OS
%ROS positive cells among neutrophils
**
Ctl OS
n=13
g
Isolation of neutrophils
Untreated or OS cells
12h of Co-culture
1 HMEC : 5 Neutrophils
Degranulation markers (CD18/CD11b/CD63)
Activation marker (PD-L1/ICAM1)
CD18
CD11b
CD63
CD274/PD-L1
CD54/ICAM1
αIso Ctl
αIso OS
αTARGET Ctl
αTARGET OS
Median of Fluorescence Intensity (MFI)
CD18 **
CD11b **
CD63 *
CD274/PD-L1 **
CD54/ICAM1 **
Ctl OS
n=10
n=10
n=10
n=9
n=9

Figure S4

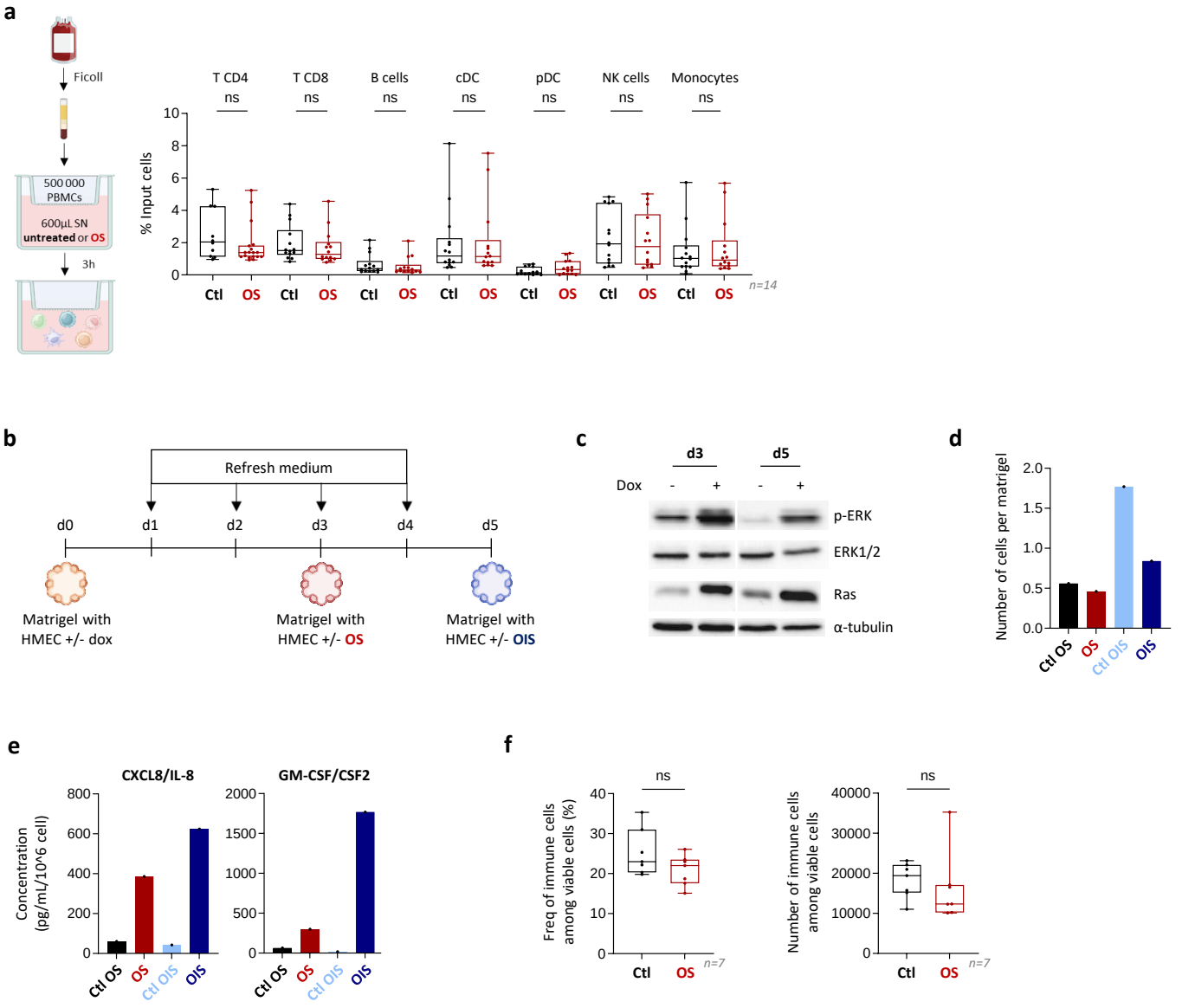
a
Ficoll
500 000 PBMCs
600µL SN untreated or OS
3h
T CD4
T CD8
B cells
cDC
pDC
NK cells
Monocytes
ns
% Input cells
Ctl
OS
n=14
b
Refresh medium
d0
d1
d2
d3
d4
d5
Matrigel with HMEC +/- dox
Matrigel with HMEC +/- OS
Matrigel with HMEC +/- OIS
c
d3
d5
Dox
p-ERK
ERK1/2
Ras
α-tubulin
d
Number of cells per matrigel
Ctl OS
OS
Ctl OIS
OIS
e
CXCL8/IL-8
GM-CSF/CSF2
Concentration (pg/mL/10^6 cell)
f
Freq of immune cells among viable cells (%)
Number of immune cells among viable cells
n=7

Figure 5

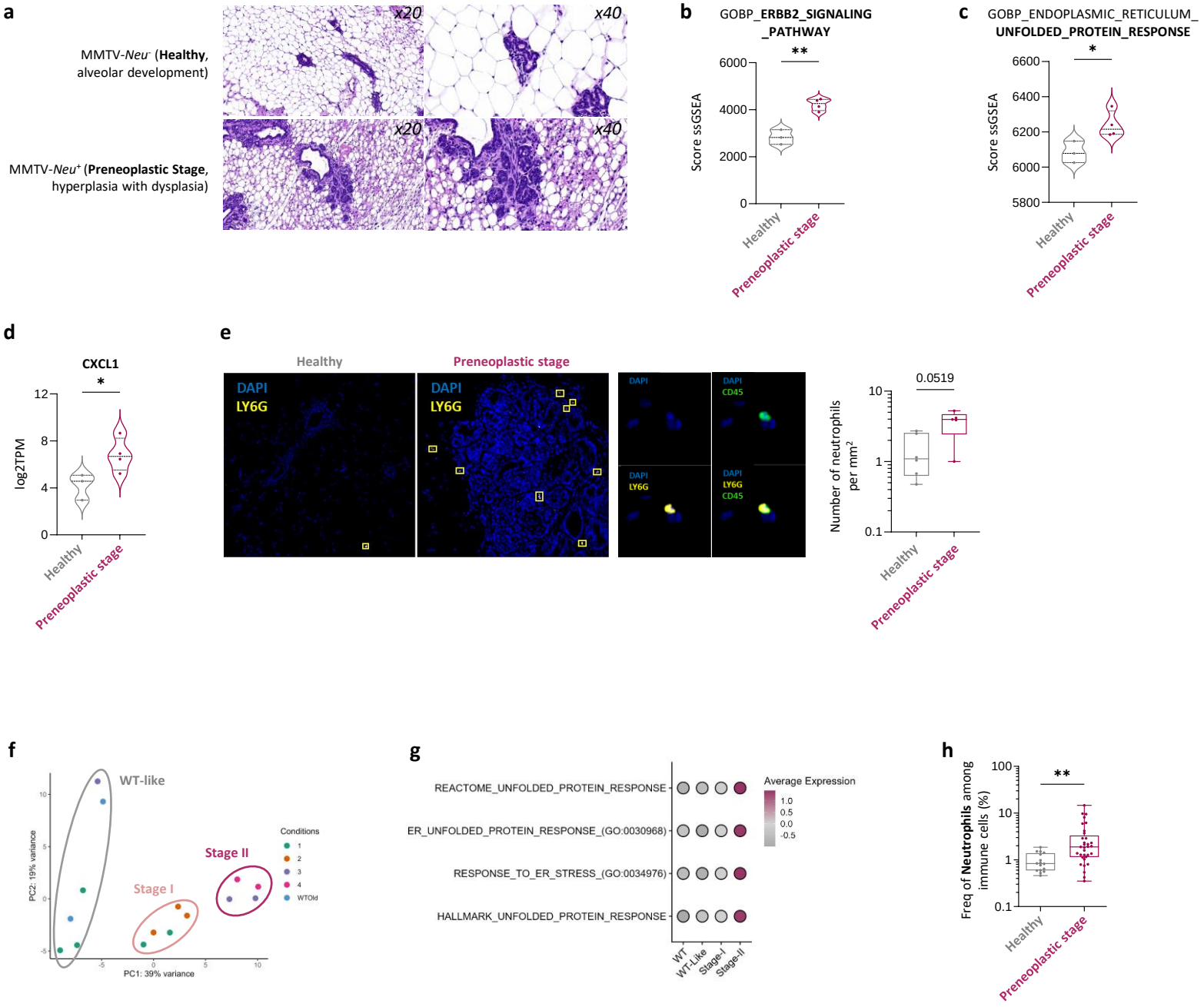
a
MMTV-Neu⁻ (Healthy, alveolar development)
MMTV-Neu⁺ (Preneoplastic Stage, hyperplasia with dysplasia)
x20
x40
b
GOBP_ERBB2_SIGNALING_PATHWAY
Score ssGSEA
Healthy
Preneoplastic stage
c
GOBP_ENDOPLASMIC_RETICULUM_UNFOLDED_PROTEIN_RESPONSE
Score ssGSEA
d
CXCL1
log2TPM
e
Healthy
Preneoplastic stage
DAPI
LY6G
CD45
Number of neutrophils per mm²
0.0519
f
WT-like
Stage I
Stage II
Conditions
PC1: 39% variance
PC2: 19% variance
g
REACTOME_UNFOLDED_PROTEIN_RESPONSE
ER_UNFOLDED_PROTEIN_RESPONSE_(GO:0030968)
RESPONSE_TO_ER_STRESS_(GO:0034976)
HALLMARK_UNFOLDED_PROTEIN_RESPONSE
Average Expression
WT
WT-Like
Stage-I
Stage-II
h
Freq of Neutrophils among immune cells (%)

Figure S5

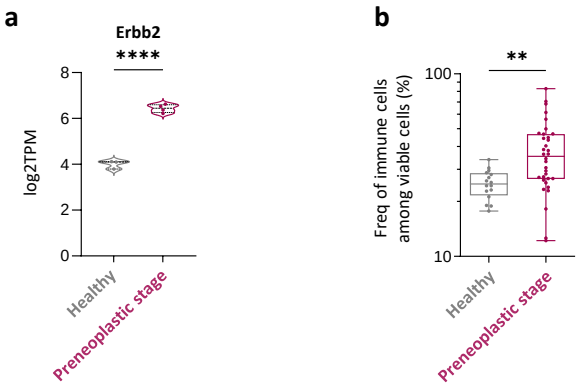
a
Erbb2
****
log2TPM
8
6
4
2
0
Healthy
Preneoplastic stage
b
**
Freq of immune cells among viable cells (%)
100
10
Healthy
Preneoplastic stage